Physics – Uspekhi **56** (10) 973 – 998 (2013)

REVIEWS OF TOPICAL PROBLEMS PACS numbers: **36.40.–c**, 36.40.Ei, 64.70.D–, 71.15.Mb, 81.16.Hc, **82.30.–b**

Modeling of configurational transitions in atomic systems

R S Berry, B M Smirnov

DOI: 10.3367/UFNe.0183.201310b.1029

Contents

Abstract. **Configurational transitions in atomic systems, i.e., transitions that change the system's geometric structure, include chemical reactions in gases, transitions between aggregate states of a polyatomic system, i.e., the phase transitions, and nanocatalytic processes. These transitions are analyzed from the standpoint of the behavior of the system on its effective potential energy surface (PES), so that the transition results from passage between different local minima of the PES. It is shown that the density functional theory (DFT) is suitable, in principle, for the analysis of complex atomic systems, but this method, being based on contemporary computer codes, is not suitable even for simple atomic systems, such as heavy atoms or metal clusters. Next, a statical determination of the energetic parameters of atomic systems does not allow analyzing the dynamics of configurational transitions; in particular, the activation energy of a chemical process differs significantly from the height of a potential barrier which separates the atomic configurations of the initial and final states of the transition. Notably, the static models, including DFT, give a melting point for clusters with a pairwise atomic interaction that is twice that from dynamic models which account for the thermal motion of atoms. Hence, the optimal description of configurational transitions for complex atomic systems may be based on joining the DFT methods for determining the PES of this system with molecular dynamics to account for the thermal motion of atoms.**

R S Berry Department of Chemistry, University of Chicago,
929 East 57th St., Chicago, IL 60637, USA
E-mail: berry@uchicago.edu
B M Smirnov Joint Institute for High Temperatures,
Russian Academy of Sciences,
Izhorskaya ul. 13/19, 127412 Moscow, Russian Federation
Tel./Fax +7 (499) 190 42 44
E-mail: bmsmirnov@gmail.com

Received 21 January 2013, revised 6 April 2013
Uspekhi Fizicheskikh Nauk **183** (10) 1029 – 1057 (2013)
DOI: 10.3367/UFNr.0183.201310b.1029
Translated by B M Smirnov; edited by A Radzig

1. Introduction

Contemporary developments in physics are ever more connected to progress in computer technology, whose throughput opens new possibilities for the description of physical objects and phenomena. This paper is devoted to clusters, systems of finite, not-very-large numbers of atoms, and some processes involving those clusters, mostly their phase transitions and catalytic processes. We shall largely consider the properties and evolution of a cluster on the basis of its potential energy surface (PES) [1], which is constructed in a multidimensional space of nuclear coordinates of cluster atoms, by applying the Born–Oppenheimer approximation which allows us to assume that the electrons of the system come to a stable, equilibrated state, whatever the geometric arrangement of the nuclei may be. The cluster's evolution corresponds, in this picture, to displacement of a representative point along a path on the PES in a space of nuclear coordinates. A principal characteristic of a cluster's PES is the existence of a large number of local minima [2–4] which characterize stable and metastable states of clusters as systems of bound atoms. Consequently, the cluster's evolutionary path consists of a chain of transitions between local minima of the PES which are separated by potential barriers [5, 6]. This characterization of cluster evolution, the saddle-crossing dynamics [7, 8], has proven to be the most reliable and successful method for analyzing cluster evolution [9].

Let us draw attention to the following fact. Assuming that the atomic motion is governed by a classical law, we can

completely describe the motion of a representative point in the phase space, i.e., in a space of nuclear coordinates and momenta. Whereas, cluster evolution described as motion along a trajectory on the PES gives only a part of the picture, because this approach excludes much of the nuclear motion, particularly the small-amplitude vibrations. But because of cluster compactness, a strong interaction between neighboring atoms leads to establishing thermodynamic equilibrium of those vibrations in this atomic system. One can divide the cluster's degrees of freedom into configurational and thermal ones, i.e., those responsible for small-amplitude vibrational motions. These two classes of degrees of freedom are largely separable [10]. In this case, the vibrational motion of the atoms can be characterized by a temperature T which is associated with the average kinetic energy of clusters. Hence, in describing cluster evolution as a motion along a PES, it is generally necessary to assign a specific temperature to the cluster.

Let us consider the method we will use to construct a cluster's PES. The simplest example corresponds to a pairwise atomic interaction in clusters, e.g., with the popular Lennard-Jones atomic interaction potential [11, 12]. Although this interaction is not suitable even for a precise representation of inert gases [13], this model potential does contain simultaneously short-range and long-range parts. Another class of empirical potentials is useful for metal clusters (see, for example, Refs [14–20]). The shape of the appropriate interaction potential depends, of course, on the cluster material. The use of effective interaction potentials is reliable and efficient, because parameters of whatever interaction potential are adjusted to fit the observed properties of the macroscopic metal in question.

However, the most elaborate and widely used method for describing cluster behavior has its roots in the density functional theory (DFT) [21, 22]. In this approach, bilinear functionals are used rather than electronic wave functions for determining the average energy of the system of interacting atoms as a quantum system at a given nuclear configuration. The advantage of this method is the variation principle [21], which allows us to choose optimal parameters for a given functional form. DFT is a universal method for cluster description [23–28], and computer programs are available for the application of this method. However, despite the above merits of DFT, the following limitations accompany this method. First, as based on the variation principle, DFT relates only to the ground electronic state of an atomic system. Hence, it is not suitable in the standard form for catalytic processes in which different electronic states are involved. Second, the nuclei in this quantum problem are motionless, and the results in the first approximation relate to zero cluster temperature.

The latter limitation may be removed if static DFT is joined with the molecular dynamics method (MDM) under the assumption of classical motion of nuclei. MDM allows one to take into account the dynamics of atomic motion in a bound system of atoms. This method accounts for the motion of each nucleus (atom) in a system of interacting atoms [29–32]. Although a system of interacting atoms is a determinate one within the framework of MDM, because this method includes trajectories for each atom under the given conditions, in reality this method is a statistical one because of the development of Poincaré instability from small uncertainties in atomic positions, including uncertainties resulted from the use of numerical methods for describing the system. For a system of classical atoms, MDM is sufficiently well grounded for providing the analysis of nonequilibrium systems of interacting atoms [33–37].

Computer codes (see, for example, Refs [38–41]) facilitate the wide use of this method. The combination of the static DFT method for describing interactions in an atomic system and MDM for describing the atomic dynamics for the analysis of solids is known as the Car–Parinello method [42]. In particular, this method allows one to analyze the phonon spectra of solids. Methods based on model interaction potentials in metal atomic systems have proved to be more practical and reliable for a description of metal clusters than traditional DFT. But such model methods are not suitable for describing more complex atomic systems where DFT must be applied. In these cases, it is difficult to determine the accuracy and reliability of DFT evaluations, especially the numerical parameters of atomic systems.

Atomic systems of various complexity and processes proceeding in these systems are the topic of this paper. These processes include chemical reactions involving simple molecules, phase transitions, and nanocatalysis. Our task is to show that processes in these and other atomic systems proceed through transitions between configurational states, and that the experience accumulated in executing the analysis of these systems gives a useful information about some aspects of these processes in more complex systems.

2. Chemical processes involving gaseous molecules as configurational transitions

2.1 Configurational transitions as characteristic of the evolution of an atomic system

Our goal is to formulate a reliable method for modeling a complex atomic system in the way that reveals the character of its evolution. For this purpose, we begin by establishing some physical concepts. The first of these is the Born–Oppenheimer approximation, which allows us to separate the electronic degrees of freedom from those due to nuclear motion. Within the framework of this approximation, we first consider the simplest atomic system consisting of only two atoms. Since typical electronic times are very short compared to those of nuclear motion, electrons follow nuclear motion, equilibrating rapidly with every change in the nuclear positions, and the electron distribution at any configuration of nuclei is identical to that for motionless nuclei in that geometry. The Born–Oppenheimer approximation is valid for the configurational dependence of the electronic energy for the excited electronic states, as well as for the ground state. The electronic energy for each internuclear distance gives the electron terms of the atomic system.

Slow atomic collisions may leave the system in its initial electronic state, or may involve an electronic transition to another electron term [43]. If the electronic energy is at or near a local minimum, corresponding to a potential well, this may well give rise to vibrational motion of the nuclei. Hence, the degrees of freedom in the region of a geometrically stable molecule fall into two separable classes, electronic modes and nuclear modes, which for a diatomic molecule are just the single vibrational and rotational nuclear motions.

Let us move on to a more complex system consisting of several atoms. Then the electronic energy for each electronic state depends on all the nuclear coordinates, i.e., on the

nuclear configuration, so the electronic energy is a function of all the nuclear coordinates for any given electronic state. That configuration-determined energy is precisely the PES. Let us now analyze the PES for the simplest polyatomic system consisting of three hydrogen atoms. We focus first on the linear geometry. In this case, the PES depends on just two variables: the distances of the middle atom to each outer atom. If one of those distances is sufficiently long, the system comprises really a hydrogen atom and a hydrogen molecule with a single chemical bond; the system really has only one H–H bond. Ignoring a weak long-range attraction between this atom and molecule, we obtain two minima of the PES which correspond to the atom and molecule at large separations, and the chemical bond of the middle atom can be realized with either outer atom. Since the approach of the atom and molecule is accompanied by their repulsion, the PES in a two-dimensional space is characterized by two local minima, 'valleys', separated by a potential barrier. The potential barrier height corresponds to the activation energy for the transition between the PES minima. (Strictly speaking, the activation energy and the barrier height are not precisely equivalent, because the latter depends only on the potential surface, and the activation energy also depends on the vibrational energy in the bound pair of atoms.) Hence, this example illustrates how the change in nuclear configuration in collisions of atoms and molecules relates to chemical reactions in gases, and the analysis of these processes allows us to understand some peculiarities of configurational transitions.

A cluster, i.e. the system of a finite number of bound atoms or molecules, is a more complex system. We demonstrate a configurational transition for the example of a 13-atom cluster for which the interactions occur predominantly between nearest neighbors. In the ground configurational state this cluster has an icosahedral structure, as shown by the solid lines of Fig. 1; the configurational transition occurs via an atom moving from the filled outer atomic shell to the cluster's surface, as shown by the dashed lines and arrows. This case allows one to visualize the transition from the solid, closed-shell state to the lowest configurational state that could be considered liquid. Of course, further promotions release more atoms to weakly constrained positions analogous to that of a single atom promoted in Fig. 1. If we estimate the cluster's energy in this case by counting the number of chemical bonds between nearest neighbors, this lowest transition is accompanied by a loss of three bonds, because the atom executing transition has six bonds with nearest neighbors when it resides in the outermost atomic shell, whereas it acquires only three bonds in its promoted site on the cluster surface. This example characterizes one more aspect of cluster configurational transitions, in that they correspond to transitions over the potential barrier at saddles separating local minima of the PES, namely the saddles bearing responsibility for configurational transition states. Indeed, in the course of the transition between the two local potential wells in Fig. 1, the promoting atom has only two nearest neighbors at the saddle, and thus only two bonds, and hence we know the energy of the transition state.

Next, we designate the lowest configurational state in this simple example as the solid aggregate state, and the upper transition state as the liquid (meaning, of course, the lowest configurational state of the liquid, since many more states become accessible when the cluster acquires more energy). The definition of the solid and liquid aggregate states of

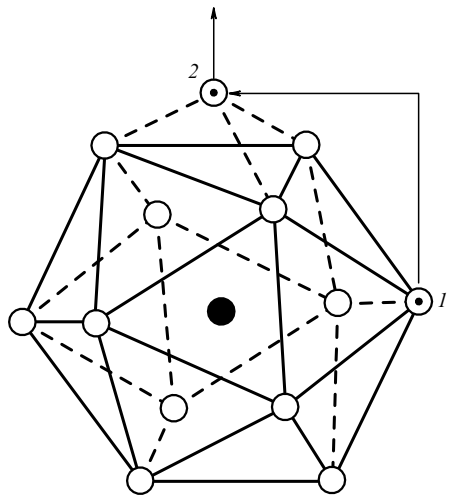

Figure 1. Transition from the ground configurational state to the lowest excited configuration for a cluster of 13 atoms [44], in which interaction between nearest neighbors dominates. In the ground configurational state, this cluster has an icosahedral structure. The transition under consideration transfers an atom of the surface atomic shell (position *1*) to the cluster surface (position *2*), leaving the system with one promoted particle and a vacancy in the icosahedron.

macroscopic atomic systems in terms of the long-range character of the symmetry is not suitable for small systems such as atomic clusters. The appropriate basis for defining the phases of such small systems may be the typical time of survival of a given configuration. Thus, for changing the ground atomic configuration, two cluster atoms must exchange sites, which is a very slow process, whereas a configurational change even in that first promoted configuration involves either the passage of the promoted atom from one surface location to another or moving of the hole left in the icosahedral shell to a different site. It is clear that survival times of the lowest and first excited configurational states are very different, i.e., the atomic diffusion coefficients for these states differ significantly. Therefore, if the time scale of the promoted state is short compared to that of the lowest state, we recognize the upper configurational state to be fluid, and the lowest state to be a stable solid-like state.

Note that in introducing the concepts of solid and liquid aggregate states for clusters in Fig. 1, we implicitly used thermodynamic concepts. We are now moving to a visually based or mobility-based definition of the liquid state instead of the traditional one. Therefore, we give below a different definition of the liquid state for a system of a finite number of bound atoms, and we will show why one can consider excited configurational states of the kind illustrated in Fig. 1 as the liquid state. Another closely related way to define the solid and liquid states is in terms of the extent of fluctuations in atomic motion. This approach was first introduced by Lindemann [45], who used the relative root-mean-square fluctuations of atom positions from their equilibrium positions. Then this criterion was modified having regard to the fluctuations of interparticle separations as the criterion [46–48]. If the fluctuations are less than 10% of their mean, the system is deemed solid. Typically, there is a jump from a value well below 10% to something significantly larger, when the atomic system 'melts'.

Associated closely with the fluidity of the atomic system in its liquid state is the condition that the latter exhibits a high

entropy because of the variety of configurations accessible to it. More specifically, if the entropy is evaluated on a time scale that is long compared to local vibrations, long enough for the system to explore its energetically accessible regions on the potential surface, we can define the state as encompassing all accessible excited configurations. Then the statistical weight of the group of excited configurational states for the single promotion of Fig. 1 is $g = 12 \times 15 = 180$ (the product of the number of hole positions by the number of promoted atom positions on the cluster surface). The configurational entropy is, of course, the natural logarithm of this statistical weight. The cluster can occupy a given excited state starting from some temperature. In this manner, some configurational states may be identified with the aggregate states of an atomic system, and transitions between such states are phase transitions.

We now consider the configurational states of Fig. 1 from the standpoint of behavior on the PES. Evidently, the first and last of them correspond to local minima of the PES, and one can describe motion of nuclei near the PES minima as approximately harmonic. So long as nuclear motion can be treated as a sum of harmonic oscillations, the vibrational and configurational degrees of freedom are separable. But this separation becomes invalid when the nuclear vibrational degrees of freedom get essentially more excited. When this happens, it becomes incorrect to describe configurational transitions in terms of the PES alone: one must include the contribution from nuclear motion. In other words, the height of the potential barrier separating two configurations does not coincide with the effective activation energy characterizing the transition rate between these states. Thus, in modeling the transition between configurational states of an atomic system, it is necessary to extend the static description based strictly on the topography of the PES to include the contribution of the dynamical.

2.2 Peculiarities of chemical processes in molecular collisions

Let us consider the process of molecular collision that leads to the change in the chemical composition of two colliding molecules via the reaction

$$AB + CD \to AX + CY\,, \tag{2.1}$$

where A, B, C, D, X, Y are atoms or radicals which do not change their configuration in the course of the chemical reaction. We specifically consider chemical processes for which the initial and final states of reactant and product molecules occupy their ground electronic states. That allows us to describe the chemical process (2.1) as a result of the evolution of the total system along the single PES of the ground electronic state of the 4-element system. Let us assume that DFT or a simplified version of it enables us to construct the PES for the system of colliding molecules, and it is possible, at least for zero nuclear temperature. Then the chemical process is a result of a transition between local minima of the potential surface which correspond to the initial and final molecular states involved in the process. Hence, to determine the rate constant of this process, we first construct the full PES and then express the rate of the chemical process through its parameters. This is a general method which we apply in the analysis of chemical processes and which is a basis for the numerical analysis of complex chemical processes.

One can assume this scheme to be valid for molecules for which the ground electronic state is separated from the lowest excited state by a wide energy gap. However, this method does not hold true for metal particles, say, for processes involving metal clusters. But this need not be a barrier to our description of the kinetics of the processes. Indeed, electronic excitation of a metal system can be described as a continuous process involving a transition within an incomplete energy band of electronic states. Recognizing that electronic and configurational states may be separated in a metal atomic system, we arrive at an analogy between chemical processes proceeding in metal and dielectric systems. Of course, because of a nonzero electronic temperature, the electronic state of a metal system may be an excited one, but assuming that the variation of the electronic excitation energy is small within the range of the thermal energy of the electrons, it turns out that the above analogy holds true.

Traditionally, the rate of a chemical process (2.1) is determined by the height of the energy barrier for the process, and this barrier height is typically large compared with the thermal energy of atoms or molecules. Then, the rate constant of a chemical process is given by the Arrhenius formula [49]

$$k_{\mathrm{ch}} = A \exp\left(-\frac{E_{\mathrm{a}}}{T}\right), \tag{2.2}$$

where T is the molecular temperature expressed in energy units, the activation energy of the chemical process E_{a} is connected with the barrier height, and the pre-exponent A corresponds to averaging the particle velocities over collision trajectories with a thermal distribution of atoms at the chosen temperature. Under this assumption, $E_{\mathrm{a}} \gg T$, the activation energy corresponds to a minimum energy for the process as the system evolves along the PES of its ground electronic state.

Thus, within the framework of the process under consideration we divide the problem into two parts for numerical simulation. At first stage, we find the PES of the total atomic system of colliding molecules; at the second stage, we analyze the dynamics of this process as motion along optimal trajectories on this PES. For noncomplex systems, some elements of this analysis can be simplified, thus allowing us to understand the role of elementary factors in a specific chemical process. Therefore, we first consider simple cases of chemical processes and configurational transitions which have been studied in sufficient detail, regardless of the general scheme.

2.3 Chemical processes involving hydrogen atoms and molecules

We consider below the simplest chemical process which has been studied in detail and proceeds according to the scheme

$$\mathrm{H(D)} + \mathrm{H_2} \to \mathrm{H_2(HD)} + \mathrm{H}\,, \tag{2.3}$$

where the parentheses are meant to indicate that one of hydrogen atoms may be replaced by its isotope — a deuterium atom. This process can be described by the classical laws of the atomic motion. A significant simplification of this problem results from the fact that the maximum efficiency of this process occurs in collisions in which the three hydrogen atoms are located virtually along the same line. Then, the relevant reduced PES is described simply by the two distances R_1 and R_2 between the middle and outermost atoms.

Let us construct the PES of the collinear H_3 system. Assuming the nuclear masses to be infinite with respect to the electron mass, we find the energy of three electrons placed in the field of three Coulomb centers as a function of the distances between these centers. We suppose that the hydrogen atoms are in their ground states at infinite separation. The electronic terms of the ground state of this system or the PES as a function of R_1, R_2 are plotted in Fig. 2 and Fig. 3, in accordance with calculations [50]. Figure 2 displays the dependence of the electronic energy on the distance R_1, when the distance R_2 is fixed, and Fig. 3 contains equipotential curves of this system in the frame of R_1- and R_2-axes. It should be noted that the electronic energy of this system is conserved under the exchange operation $R_1 \leftrightarrow R_2$, so that equipotential curves in Fig. 3 are symmetric with respect to the line $R_1 = R_2$, and thus Fig. 3 shows only the part $R_2 \geqslant R_1$ of the electronic energy. Note that at the distance 1.75, there is a symmetrical stationary point.

These results of numerical PES calculations for the ground state of the system of three hydrogen atoms allow one to understand the character of the interactions in this system. The local minima of the PES correspond to the formation of a chemical bond of the middle atom with one of the outer atoms. Each of these local minima has the form of a valley in a space R_1, R_2; these valleys are separated by a potential barrier whose height is approximately 0.4 eV. Then, the chemical process (2.3) leading to replacement of the chemical bond of the middle atom with one atom by the bond formed with another atom corresponds to a transition over the barrier from one valley to the other.

Let us analyze the approximation we have just used. The basis for our analysis is the Born–Oppenheimer approximation or the adiabatic concept of molecular physics, which holds true if nuclear velocities are small compared with typical electron velocities. This assumes that the spatial distribution of electrons redistributes essentially instantaneously during any movement of the nuclei. This implies that there is always a self-consistent field in which the nuclei are moving. In the theory of atomic collisions, the slowness of nuclear motion is described by the Massey criterion [51]:

$$\xi = \frac{a\Delta E}{\hbar v} \gg 1\,. \tag{2.4}$$

Here, ξ is the Massey parameter; a is a typical internuclear distance at which a change in the electron distribution and electronic wave function comes into prominence by approaching a detectable amount, an amount that should be used in the description of atomic collisions; ΔE is a typical change in energy for this process that equals the barrier height for the chemical process of the type (2.3), and v is a typical nuclear velocity. The Massey criterion (2.4) forms the basis for the processes under consideration, starting from atomic collisions [43, 52, 53] and chemical processes similar to reaction (2.3) and finishing with processes of structural change for clusters and macroscopic atomic systems. Additionally, in the subsequent discussion we assume the classical character of nuclear motion in the self-consistent field of the electron system.

Let us consider the chemical process (2.3) from another standpoint, as the transition between electronic states of the system of three hydrogen atoms. Using the one-electron approximation, we represent the basis wave functions Ψ_1, Ψ_2 of the system of three hydrogen atoms in the form of the Slater determinants [54–56], which takes into account the symmetry with respect to exchange of two electrons. The

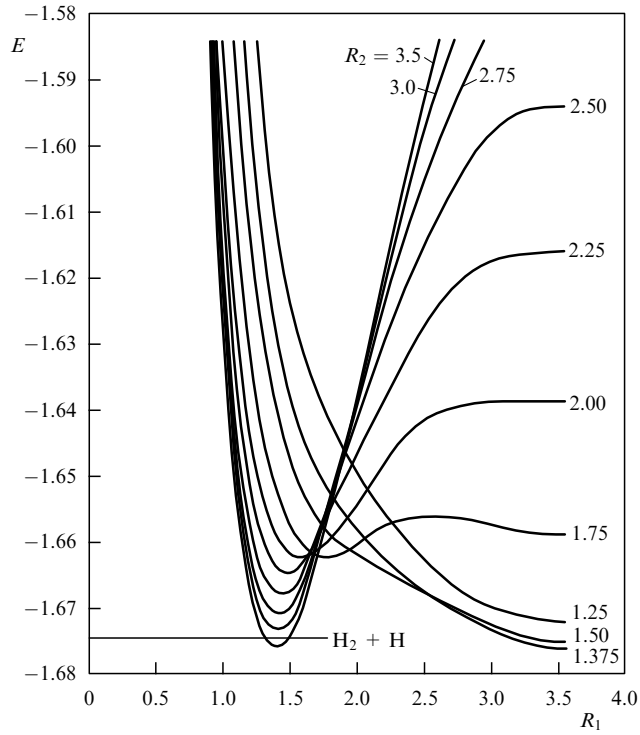

Figure 2. Dependence of the potential energy E for a system of three hydrogen atoms located along a line as a function of the distance R_2 between the middle and right outermost atoms, with the distance R_1 between the middle and left outermost atoms fixed [50]. Distances R_1 and R_2 are expressed in the Bohr radius a_0, the potential energy is given in atomic units, and the zero energy corresponds to an infinite distance between nuclei of the H_2 molecule and the free atom.

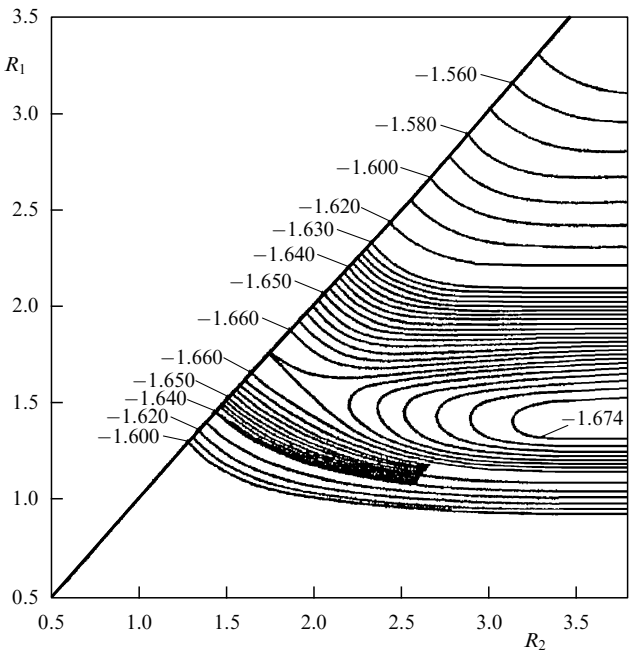

Figure 3. Equipotential lines for a system of three hydrogen atoms positioned on a line in the frame of reference whose axes are the distance R_2 between the middle and right atom and the distance R_1 between the middle and left atom [50]. Due to the symmetry, the substitution of the ordinate for the abscissa does not change the positions of the equipotential curves. Distances R_1 and R_2 are expressed in the Bohr radius a_0, the potential energy is given in atomic units, and the zero energy corresponds to infinite distances between nuclei, i.e., to three free atoms.

eigenfunctions of the system of three hydrogen atoms are then a combination of basic wave functions Ψ_1, Ψ_2 having the following form:

$$\Psi_1 = \begin{vmatrix} \varphi_a(1)\,\eta_-(1) & \varphi_b(1)\,\eta_+(1) & \varphi_c(1)\,\eta_+(1) \\ \varphi_a(2)\,\eta_-(2) & \varphi_b(2)\,\eta_+(2) & \varphi_c(2)\,\eta_+(2) \\ \varphi_a(3)\,\eta_-(3) & \varphi_b(3)\,\eta_+(3) & \varphi_c(3)\,\eta_+(3) \end{vmatrix}, \qquad (2.5)$$

$$\Psi_2 = \begin{vmatrix} \varphi_a(1)\,\eta_+(1) & \varphi_b(1)\,\eta_+(1) & \varphi_c(1)\,\eta_-(1) \\ \varphi_a(2)\,\eta_+(2) & \varphi_b(2)\,\eta_+(2) & \varphi_c(2)\,\eta_-(2) \\ \varphi_a(3)\,\eta_+(3) & \varphi_b(3)\,\eta_+(3) & \varphi_c(3)\,\eta_-(3) \end{vmatrix}. \qquad (2.6)$$

Here, indices a, b, c refer to nuclei which form a certain configuration, η_+, η_- are the electron spin wave functions for an indicated projection of the electron spin onto a given direction, and the argument gives the index number of the electron described by each coordinate function φ. We use identical spatial wave functions φ of electrons, with each centered on its own nucleus. We restrict ourselves to describing this atomic system at a fixed spin direction of one electron opposite to the spin direction of the two other electrons in order to represent the formation of a chemical bond. In contrast, if the three spins are parallel, there would be no chemical bond between atoms.

The wave functions (2.5), (2.6) lead to different spatial distributions of electrons for this atomic system. One can construct the electronic eigenfunctions of a system of three electrons in the field of three Coulomb centers from these wave functions. In particular, if an atom and molecule participating in process (2.3) are in their ground electronic states, two electronic states can characterize the interacting atom and molecule, and process (2.3) is responsible for the transition between these two states. In the course of this transition, a spatial redistribution of electrons occurs. A schematic distribution of electrons is given in Fig. 4 for the states described by wave functions (2.5) and (2.6). Although these wave functions are not the true eigenfunctions for the system of three hydrogen atoms, one can expect that the transition between these two electronic states is accompanied by an electron transfer. This gives two types of transitions in the system of interacting atoms: the first results from a change in the nuclear configuration, whereas the second is connected with a change in the spatial distribution of the electrons.

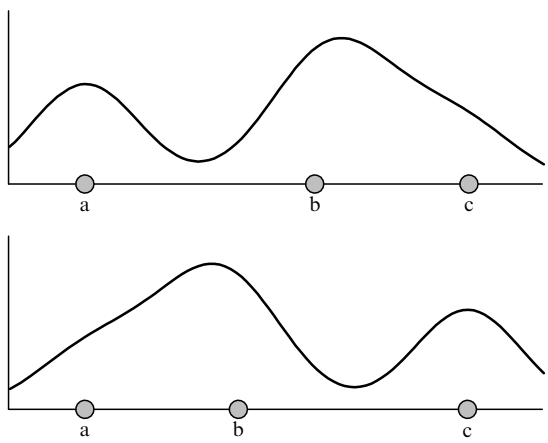

Figure 4. Schematic distribution of the electron density for two states of a system of three hydrogen atoms in the ground electronic state, where nuclei are aligned along the same line and the electron wave function is a combination of the wave functions (2.5) and (2.6).

2.4 Dynamics of chemical processes involving hydrogen atoms and molecules

Process (2.3) is the simplest chemical reaction whose analysis [57–60] set a classic example of the theoretical description of chemical processes based on examining the behavior of colliding molecules on a PES. A general approach was developed proceeding on the theory of this process for the analysis of other, more complex processes [61–64]. Within the framework of this general approach, a chemical reaction is considered as a transition between minima of the PES for a system of interacting molecules or atoms, with their relative motion typically described classically. We next focus on process (2.3) and ascertain its reliability to yield the cogent parameters of this reaction on the basis of the parameters of the PES for the system of three hydrogen atoms.

We show first the validity of the assumption that the main contribution to the rate of this process comes from collinear atomic collisions. Figure 5 gives the dependence of the rate of process (2.3) on the angle between the axis of the hydrogen molecule and a line joining the hydrogen atom and the nearest atom of the hydrogen molecule. Figure 5 corroborates the validity of this assumption.

One can expect that the activation energy E_a for the chemical process correlates with the height E_b of the potential barrier which separates local minima of the PES corresponding to the initial and final states. Let us compare these energies for process (2.3). The barrier height of the

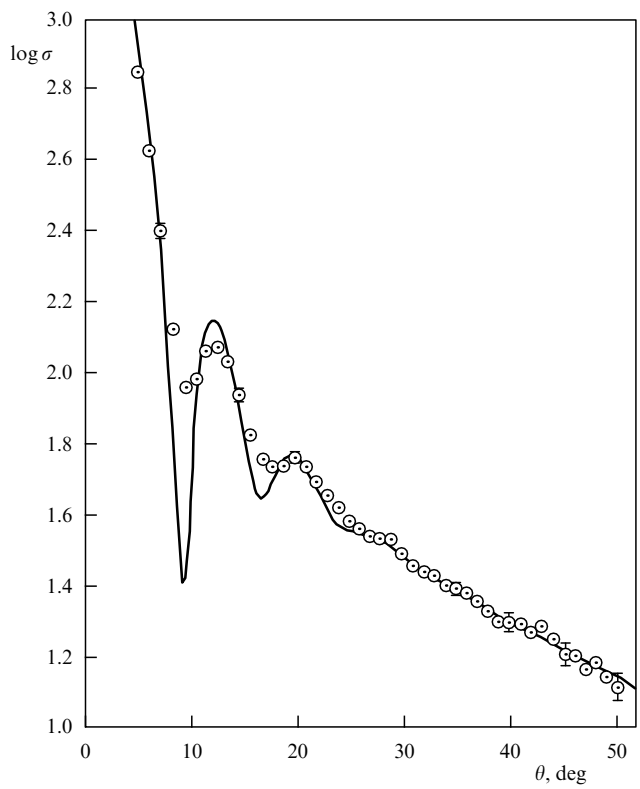

Figure 5. Relative cross section of process (2.3) as a function of the angle θ between trajectories of motion of outermost atoms with respect to the middle one. Experimental values [65] are given by circles, and theoretical values [66] are shown by the solid curve.

PES with respect to its minima according to Ref. [67] is $E_b = 9.68 \pm 0.12$ kcal mol^{-1} $= 4870 \pm 60$ K, while according to Ref. [68], $E_b = 9.8 \pm 0.2$ kcal mol^{-1} $= 4930 \pm 100$ K. We see that these values coincide within their accuracy limits. The approximation by the Arrhenius formula (2.2) of the results of measurements [69] for the rate of process (2.3) in the temperature range $T = 300-1000$ K gives the following parameters of the Arrhenius formula: $E_a = 7.435$ kcal mol^{-1} ≈ 0.32 eV ≈ 3700 K, and $A = 4.33 \times 10^{13}$ cm^3 mol^{-1} s^{-1} $= 7.2 \times 10^{-11}$ cm^3 s^{-1}. As evident from the data received, the difference between the heights E_b of the barrier separating the relevant minima of the PES of process (2.3) and the activation energy E_a for this process is far greater than the thermal energy of the atoms, with the ratio E_a/E_b reaching approximately 3/4. The difference between these values testifies to the influence of atomic thermal motion on the rates of chemical processes. In addition, the analysis of process (2.3) within the framework of classical, quasiclassical, and quantum methods leads to similar results.

Let us compare the pre-exponent A in the Arrhenius formula (2.2) for process (2.3) with the gas-kinetic rate constant for collisions between hydrogen atoms and molecules:

$$k_g = v_T \sigma_g \,, \quad v_T = \sqrt{\frac{8T}{\pi\mu}}, \tag{2.7}$$

where $v_T = 3.1 \times 10^5$ cm s^{-1} is the thermal velocity of collisions of the hydrogen atoms and molecules at $T = 300$ K, and $\sigma_g = 1.7 \times 10^{-15}$ cm^2 [70] is the gas-kinetic cross section for these collisions, and μ is the reduced mass of colliding particles. We find from this the gas-kinetic rate constant $k_g = 5.2 \times 10^{-10}$ cm^3 s^{-1}, and the ratio between these quantities: $A/k_g = 0.14$. It follows from this small ratio that small scattering angles make the main contribution to the rate constant of process (2.3).

2.5 Character of transitions on the PES for chemical processes

The analysis of the simplest chemical processes and their portrayal in terms of transitions between local minima of the PES allows us to formulate general principles of the analysis for processes involving atomic particles and to understand the possibility of using contemporary methods of numerical simulation for complex atomic systems. We ascertain that the chemical process proceeds both as a result of change of nuclear configuration and in electron transfer from one force center to another. Let us analyze each mechanism separately.

Process (2.3) is an example of the first type of chemical processes, with transfer of a chemical bond in the collision of a hydrogen atom and molecule or their isotopes. If the hydrogen atom and molecule are in their ground states, there are two electronic states at each nuclear configuration which correspond to different combinations of wave functions (2.5) and (2.6). If the distances between the middle and outermost nuclei coincide, $R_1 = R_2$, these energies are equal. Transfer of the chemical bond in process (2.3) corresponds to transition from the space region $R_1 > R_2$ to the region $R_1 < R_2$. The potential barrier separating these regions lies along the line of $R_1 = R_2$, and the minimum barrier height is realized if the three atoms are collinear. Correspondingly, the main contribution to the transition rate comes from just those collinear collisions for which the direction of the incident hydrogen atom's velocity is along the molecular axis. We add to this that transition (2.3) includes two (degenerate) electronic states of the three-atom system. It is very helpful to use DFT for constructing the PES of the interacting hydrogen atom and molecule, since the advantages of DFT based on the variational principle relate to the ground electronic state.

Thus, if the chemical process involving gaseous atoms or molecules leads to a change in the nuclear configuration, i.e., consists in changing the character of chemical bonds, this process may be considered as the evolution of the total atomic system when it undergoes a transition between local minima of the PES, which belong to the ground electronic state. In this case, the PES of the total atomic system may be constructed and used. But the thermal motion of the nuclei affects the rate of this process, specifically via its rate constant which is not contained within the PES parameters. Hence, a suitable method for analyzing such a chemical process requires a combination of DFT (or some other counterpart) and molecular dynamics methods. This combination may be obtained within the scope of a classical analysis of the evolution of an atomic system along its PES [61–64].

Let us consider another type of configurational transitions, which is characterized by a change in the spatial distribution of electrons. This mechanism is demonstrated by the example of so-called 'harpoon reactions' [71–74], in which, during a collision of two atomic particles A and B, an electron transfers from one atomic particle to the other, according to the scheme

$$A + B \rightarrow A^+ + B^- \,,$$

and a weak interaction of the neutral particles A and B is replaced by a strong Coulomb attraction of ions A^+ and B^-. This transition typically occurs when the interatomic distance is significantly greater than the effective atomic diameters; hence the term 'harpoon'. Figure 6 shows the behavior of the electronic terms, specifically the PESs of the electronic states, and how they change roles between the long-range interaction of the ionic form and the short range interaction of the neutral atoms in this process. Let us denote by Δ the difference between the ionization potential J of a particle A and the electron affinity EA of a particle B. Then at distances $R < R_c$ between atomic particles, where the 'crossing distance' $R_c = e^2/(J - \mathrm{EA})$, the electronic energy of the ionic system $A^+ - B^-$ turns out to be lower than that of the system $A - B$ of neutral atoms. Transition of the neutral system to the state with Coulomb attraction of two oppositely charged ions in

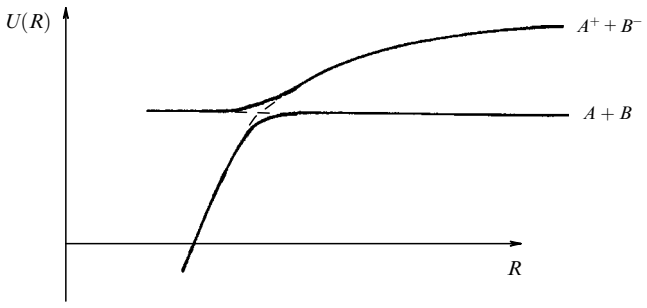

Figure 6. Behavior of electronic terms in the interaction between two neutral atomic particles A and B and their ions A^+ and B^- [75] as the basis for the harpoon reaction, i.e., for a long-range electron transfer, in collisions of these particles.

their collision, of course, restructures the chemical bonds between the atoms.

Let us demonstrate peculiarities of harpoon reactions for two examples, namely

$$\mathrm{Na} + \mathrm{F_2} \rightarrow \mathrm{NaF} + \mathrm{F} + 3.6\ \mathrm{eV}\,, \tag{2.8}$$

$$\mathrm{K} + \mathrm{Cl_2} \rightarrow \mathrm{KCl} + \mathrm{Cl} + 1.7\ \mathrm{eV}\,. \tag{2.9}$$

Systems $\mathrm{Na}^+ + \mathrm{F}_2^-$ and $\mathrm{K}^+ + \mathrm{Cl}_2^-$ represent intermediate states for these processes. The crossing of the electronic energies, i.e., of the PESs, takes place at interparticle distances $R_\mathrm{c} = 13.2a_0$ and $R_\mathrm{c} = 13.9a_0$ for these two processes, respectively. These distances yield the cross sections of these two processes: $\sigma_\mathrm{c} = \pi R_\mathrm{c}^2 = 1.5 \times 10^{-14}\ \mathrm{cm}^2$ and $\sigma_\mathrm{c} = 1.7 \times 10^{-14}\ \mathrm{cm}^2$, respectively, which are, of course, significantly larger than typical cross sections of colliding neutral particles.

Let us consider the harpoon reaction using DFT to construct the electronic terms or the PES for a system of colliding particles. We now have to deal with two electronic states which correspond, respectively, to two neutral atoms A and B and to their ions A^+ and B^-. In a pure single-state treatment, these surfaces would cross, and there would be no electron transfer. However, if the electronic wave functions of the two states are used as a basis set for the full system and because the states have the same symmetry, the ionic and neutral states mix, so that the noncrossing rule is satisfied within the Born–Oppenheimer approximation for infinitely slowly approaching atomic particles, and the lower-energy electronic term or surface, corresponding to neutral species at long interparticle distances, goes over to that of ions at distances shorter than R_c, while the upper term becomes that of neutrals there. This behavior exhibits itself in the reactions considered above and in most collisions of alkali atoms with halogen atoms.

Thus, evaluating the interaction between particles within the Born–Oppenheimer approximation leads to replacement of the intersection of terms by an 'avoided crossing' (see Fig. 6): an energy gap appears between two electronic terms of the system of interacting atomic particles. Therefore, if the distance R between particles decreases in the course of their collision, the system may remain on the lower term if the gap is large enough. In this case, DFT based on the variational principle is suitable for constructing both the lower and upper electronic terms or PESs.

Hence, one can apply the DFT method to construct the appropriate PESs for both types of configurational transitions: between local minima of a PES and those involving electron transfer; these transitions proceed via a continuous change in the nuclear configuration. But another scenario is also possible in which the excited $A^+ - B^-$ state is formed at distances exceeding R_c, and the subsequent evolution of this system results from the development of this state. This scenario is possible for catalytic processes involving, for example, long-range charge transfer; in that case, DFT must be modified because this state is excited. The important point to recognize here is that the crucial physical change, a charge transfer, occurs at a distance R considerably greater than typical atomic values.

There is one interesting apparent violation of this curve-crossing behavior, something that occurs when R_c is very large and, as a result, the transition from a neutral lower state to an ionic lower state would, within the Born–Oppenheimer picture, have to occur over a very tiny range of distances, so tiny that the atoms at real thermal velocities pass through the 'curve-crossing region' too rapidly to satisfy the Born–Oppenheimer approximation. The one example for which this violation has been established is the system Na + I [76], whose electronic spectrum reveals such a violation.

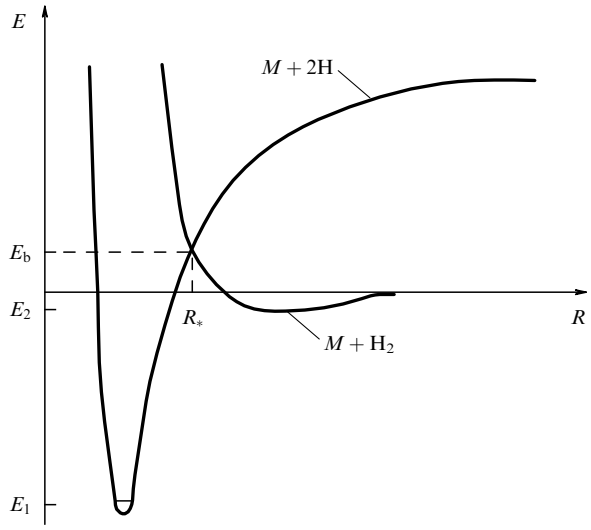

Figure 7. Electronic terms for interaction of the hydrogen molecule with a metal surface M [77].

We analyzed these chemical processes as configurational transitions between discrete states of a united system of colliding particles, so that these states characterize the initial and final states of the chemical process. But nature is more multifarious. We excluded from consideration here other processes, including those involving transitions between states lying in a continuous spectrum. Next, we reduced small metal systems to dielectric ones by accounting for only the lowest electronic state of the united system of colliding particles, neglecting low-lying electronically excited states. These simplifications lead to a loss of a variety of processes. In particular, Fig. 7 demonstrates an example of such a process and contains electronic terms for the interaction of the $\mathrm{H_2}$ molecule with a metal surface M [77]. As is seen from the diagram, at small distances R from a metal surface, dissociation of the hydrogen molecule $\mathrm{H_2}$ into atoms is energetically favorable. This means that at distances below some characteristic R_*, the bond between hydrogen atoms is broken. Thus, the more likely channel for the reaction of a hydrogen molecule $\mathrm{H_2}$ with a metal surface M is the formation of individual hydrogen atoms bonded with the metal surface.

3. Phase transitions in clusters

3.1 Phase transitions in clusters of inert gases

Phase transitions in atomic systems may be studied within the framework of classical thermodynamics [78–80] as transitions between two aggregate states. According to the thermodynamic definition, the aggregate state of a bulk atomic system is a uniform distribution of atoms in a region restricted by boundaries. In addition, the aggregate state is described by thermodynamic parameters, such as the temperature T, the entropy S, the internal energy E, and the free energy F, and also by other thermodynamic parameters [81–87]. The

phenomenological description of bulk phase transitions has a universal character contained tersely in the famous Gibbs Phase Rule, relating the number of degrees of freedom f, the number of independent components c, and the number of phases p present simultaneously in thermodynamic equilibrium: $f = c - p + 2$.

To describe the transitions between the phase-like forms of clusters as aggregate states, we assume for simplicity that such atomic systems may exhibit solid and liquid states. If the cluster (or more precisely, an ensemble of them) is in a thermostat at a temperature T and equilibrium is established both within each aggregate state and between them, the thermodynamic relation for the ratio of the probabilities of the cluster being in the liquid w_{liq} and solid w_{sol} states is given by

$$p(T) = \frac{w_{\mathrm{liq}}}{w_{\mathrm{sol}}} = \exp\left(\Delta S - \frac{\Delta E}{T}\right). \tag{3.1}$$

Here, ΔE is the energy of formation of the liquid cluster state from the solid, and ΔS is the entropy change for this transition. Let us define the cluster melting point T_{m} in its traditional manner as the temperature at which these probabilities are equal ($w_{\mathrm{sol}}(T_{\mathrm{m}}) = w_{\mathrm{liq}}(T_{\mathrm{m}})$). We then have

$$T_{\mathrm{m}} = \frac{\Delta E}{\ln g} = \frac{\Delta E}{\Delta S}. \tag{3.2}$$

Here, g is the ratio of the statistical weights of the liquid to the solid aggregate state. Thus, the phase transition is possible if the entropy change in the transition to the excited aggregate state is positive.

Here, we set as our task to determine the cluster's configurational states that correspond to local minima of the PES. These are the locally stable forms which, on suitable time scales, can attain thermal equilibrium among the small-amplitude vibrational degrees of freedom. Our vehicle for this is the simple atomic system in which interactions between nearest neighbors dominate; we will be guided by condensed inert gases. The popular interaction model for such systems is, of course, the Lennard-Jones potential [11, 12], since it includes simultaneously short-range repulsions and long-range attractions between atoms. We can safely assume that the interaction between two of these atoms is small compared to the atomic ionization potential, or even electronic excitation energies, so we can express the parameters of the system of atoms as parameters of their pair interaction potential.

Table 1 contains the reduced parameters of condensed inert gases near their triple points; the basis for these reduced parameters is the equilibrium distance R_{e} between atoms in a diatomic molecule, and the minimum of the pair interaction potential, $-D$. From these parameters and the atomic mass m one can construct any other parameter of any dimensionality. In particular, the reduced pressure is $p_0 = D/R_{\mathrm{e}}^3$, and the reduced density is $\rho_0 = m/R_{\mathrm{e}}^3$.

In this table, a is the distance between nearest neighbors, and $\rho(0)$ is the density of atoms, both at zero temperature. The differences of these reduced values from unity illustrate violations of the frequently used assumption that interactions with surrounding atoms does not influence the parameters of a test atom. Next, T_{tr} is the melting point at the triple point, p_{tr} is the pressure of the saturated vapor, $\Delta H_{\mathrm{fus}} = T_{\mathrm{tr}}\Delta s$ is the enthalpy change per atom at the triple point, Δs is the entropy change per atom there, V_{sol} and V_{liq} are the volumes per atom

Table 1. Reduced parameters of inert gases near their triple points [86, 12].

	Ne	Ar	Kr	Xe	Average
a/R_{e}	1.02	1.00	0.99	1.01	1.005 ± 0.013
$\rho(0)/\rho_0$	1.06	1.00	0.99	0.98	1.01 ± 0.04
T_{tr}/D	0.581	0.587	0.578	0.570	0.579 ± 0.007
p_{tr}/p_0, 10^{-3}	2.2	1.9	1.7	1.7	1.9 ± 0.2
$\Delta H_{\mathrm{fus}}/D$	0.955	0.990	0.980	0.977	0.98 ± 0.02
Δs	1.64	1.69	1.70	1.71	1.68 ± 0.03
$V_{\mathrm{sol}}/R_{\mathrm{e}}^3$	0.788	0.768	0.762	0.743	0.76 ± 0.02
$V_{\mathrm{liq}}/R_{\mathrm{e}}^3$	0.912	0.881	0.883	0.856	0.88 ± 0.02
$\Delta V/R_{\mathrm{e}}^3$	0.124	0.113	0.121	0.113	0.118 ± 0.006
$p_{\mathrm{tr}}\Delta V/\Delta H_{\mathrm{fus}}$, 10^{-4}	2.8	2.1	2.1	2.0	2.2 ± 0.4
$\varepsilon_{\mathrm{sub}}/D$	6.1	6.5	6.7	6.7	6.5 ± 0.3
$\varepsilon_{\mathrm{sol}}/T_{\mathrm{cr}}$	6.2	6.5	6.5	6.5	6.4 ± 0.2
$\varepsilon_{\mathrm{liq}}/T_{\mathrm{cr}}$	5.1	5.4	5.3	5.4	5.3 ± 0.1
$\varepsilon_{\mathrm{ev}}/T_{\mathrm{cr}}$	4.9	5.2	5.3	5.3	5.2 ± 0.2

for the solid and liquid states, correspondingly, and ΔV is the change in this volume at melting. We see that the change in the mechanical energy $p_{\mathrm{tr}}\Delta V$ is small at melting; this allows us to equate the change in the specific enthalpy ΔH_{fus} to the change in the internal energy ΔE for the solid–liquid phase change of condensed inert gases. In addition, $\varepsilon_{\mathrm{sub}}$ is the sublimation energy, i.e., the energy required for evaporation of one atom from the solid state of an inert gas at the triple point, and $\varepsilon_{\mathrm{ev}}$ is the energy required for evaporation of one atom from the liquid state at the triple point. The binding energy per atom in the solid ($\varepsilon_{\mathrm{sol}}$) and liquid ($\varepsilon_{\mathrm{liq}}$) states is defined by the Clausius–Clapeyron law

$$p_{\mathrm{sat}}(T) = p_{\mathrm{sol}} \exp\left(-\frac{\varepsilon_{\mathrm{sol}}}{T}\right), \quad p_{\mathrm{sat}}(T) = p_{\mathrm{liq}} \exp\left(-\frac{\varepsilon_{\mathrm{liq}}}{T}\right),$$

where $p_{\mathrm{sat}}(T)$ is the pressure of saturated vapor above the solid or liquid surface of an inert gas.

On the basis of these data, one can reach an understanding of the interactions in macroscopic inert gases and the character of their phase transitions. Note that the existence of just two aggregate states of condensed inert gases follows from our experience rather than from general considerations. Nothing in these data prevents the possibility, for example, of the existence of more than one stable solid phase. Nonetheless, based on similarity laws for the various inert gases, we conclude that these atomic systems are indeed described well by a short-range interaction between atoms, so that, effectively, only nearest neighbors interact. This yields stable crystal lattices with dense packing, specifically face-centered cubic and hexagonal lattices, with 12 nearest neighbors for every atom. Hence, the binding energy per atom is $6D$, since each atom shares half the energy of each of its bonds. That corresponds to the values of quantities $\varepsilon_{\mathrm{sub}}$ and $\varepsilon_{\mathrm{sol}}$ which characterize the specific binding energies for the solid state of inert gases. In addition, the distance between nearest neighbors in the crystal lattice at zero temperature, $a = R_{\mathrm{e}}$, also corresponds to the data of Table 1. Note that the specific

binding energy for a macroscopic system with a Lennard-Jones interaction amounts to $8.61D$ [44, 89]), and the distance between nearest neighbors is $a = 0.97R_e$; this differs from the data of Table 1 for real inert gases. It should also be noted that if we neglect the influence of atom–atom interactions on the parameters of individual atoms, values of the parameters ε_{sub} and ε_{sol} must coincide, as do parameters ε_{ev} and ε_{liq}. Indeed, averaging over various inert gases, we obtain for ratios between the above parameters: $\varepsilon_{sub}/\varepsilon_{sol} = 1.02 \pm 0.03$ and $\varepsilon_{ev}/\varepsilon_{liq} = 0.98 \pm 0.01$ [44]. Under the above assumptions, the difference between these parameters coincides with a specific enthalpy change ΔH_{fus} at melting or with a change ΔE in the specific internal energy of condensed inert gases at melting. Violation of the above equalities characterizes the error due to using the above assumption.

We now use the data for condensed inert gases to formulate what is the liquid aggregate state for an atomic system with pairwise interatomic interactions. The crystal lattice for the solid state is characterized by 12 nearest neighbors for each internal atom, corresponding to 6 bonds per atom. The transition to the liquid state reduces the number of bonds per atom by approximately one, but the volume per atom increases; that is equivalent to an increase in the statistical weight of the microstates accessible to an individual atom and, hence, to a corresponding increase in the entropy of the system. Experiments show, of course, that the liquid state is stable and is thermodynamically favored at sufficiently high temperatures.

Unfortunately, experimental data do not allow us to describe the microscopic structure of the liquid aggregate state, although one can consider it to be the result of the formation of a certain amount of free space within this atomic system. Based on this concept, and giving it a precise model by introducing an elementary void in the space between atoms, one can consider configurational excitations of the system as a result of inserting a certain number of voids into it [90–93]. The liquid state of such a system corresponds to the minimum of its free energy as a function of the void number. This allows us to construct the thermodynamics of voids which, in turn, can be based on the character of interaction between voids. This 'void thermodynamics' gives the criterion of existence of the liquid aggregate state for a macroscopic atomic system [44, 90, 94] and connects the liquid state parameters with the parameters of voids.

3.2 Phase transitions in simple clusters

Interactions in simple clusters of a single kind of atoms is analogous to interactions in bulk systems of these atoms if we ignore the surface effects. Let us first consider clusters large enough that we can use traditional bulk thermodynamic concepts for their description. From this standpoint, we analyze ground and configurationally excited states of clusters. According to formula (3.2), the stable configurational state of a cluster may be the same as its bulk aggregate state (see Section 3.1), i.e., it may be thermodynamically favored if the criterion for transition from this state, $\Delta S > 0$, holds true. However, the most stable structures of small clusters typically differ from those of the bulk. A classic example is the icosahedral structures [95] of the 'magic number' closed-shell clusters of 13, 55, 147,... atoms of rare gas atoms with interaction models based on Lennard-Jones potential. That is, the cluster configurationally excited state may be the aggregate state if its entropy (or the statistical weight per atom) is higher than that for the ground state. In this case, the cluster and bulk states are the same if the entropy of any configurationally excited state (or the statistical weight per atom) for this state is higher than that of the state with the structure of the bulk system. Therefore, clusters with completed atomic shells are convenient for demonstrating that a configurationally excited state is an appropriate model for an excited state. The cluster of Fig. 1 consisting of 13 atoms is suitable for this goal. This cluster has the icosahedral structure with fivefold symmetry [95] in its ground or solid state.

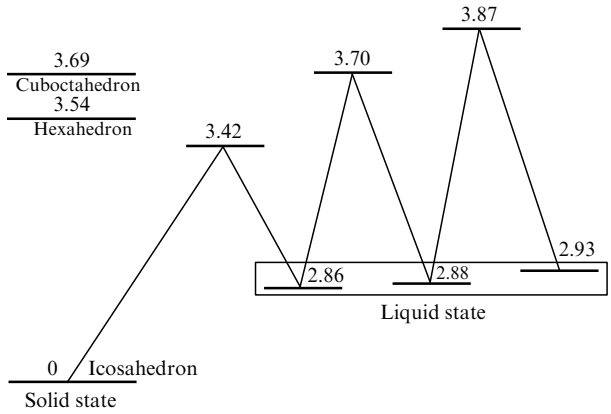

Figure 8. Energies of excitation of lower configurational states for a 13-atom Lennard-Jones cluster and energies of the potential barriers separating these states [96]. The energy to break one bond D is taken as the energy unit.

The lowest configurational excitation of this cluster corresponds to the transfer of an atom onto the cluster surface. Since this transfer leads to the loss of three bonds for a short-range interaction, the energy change is $3D$ in this transition, where D is the well depth for the interatomic pairwise interaction or the energy of breaking one bond. The long-range interaction with other atoms decreases this energy, and Fig. 8 shows the energies of excitation of configurational states and barrier energies for the transition of one atom from an external atomic shell to the cluster surface for the Lennard-Jones interaction potential between atoms. The cluster's excitation energy depends on the relative positions of the promoted atom and the remaining hole in the external atomic shell. Of course, a vacancy formed in this transition will be partially covered, but because the interactions between nearest neighbors dominate, the hole remains fixed in the former position of the promoted atom. We see that the energies of configurational excitation are similar for short-range and Lennard-Jones interactions. Naturally, atomic motion over the cluster surface is facilitated with an increasing temperature and, hence, we see that three of the configurationally excited states in Fig. 8 are joined in the cluster's liquid aggregate state.

Let us determine the statistical weight g of the configurationally excited state of the cluster depicted in Fig. 1 at zero temperature. It is the product of the number of surface cluster atoms (12) and the number of positions (15) on the cluster surface which do not border with the new vacancy, i.e., $g = 180$ and $\Delta S = \ln g = 5.2$. From this, on the basis of formula (3.2) for the melting point of a cluster with short-range interatomic interactions ($\Delta E = 3D$), we have

$$T_m = \frac{\Delta E}{\Delta S} = 0.58D\,. \tag{3.3}$$

A principal property of a cluster as a system of a finite number of bound atoms is the dynamic coexistence of the solid and liquid aggregate states [47, 97–101]. This means that within a specific range of temperatures for an isothermal cluster (or of excitation energy of an isolated cluster), the system resides in the solid state a certain fraction of the time and in the liquid state for the rest. We focus now on configurational states, and our task is to ascertain the dependence of thermal atomic motion on the parameters of the phase transition. Let us employ the results of computer simulations of an isolated 13-atom Lennard-Jones cluster [98] or of such a cluster in a thermostat [102]. These simulations allow one to determine the total energy E of cluster atoms at a given cluster temperature T for a given aggregate state. Excluding the motion of the center of mass of the 13-atom cluster as a whole, we have 33 vibrational degrees of freedom for cluster atoms, and the total average cluster energy due to thermal motion of the atoms is $K = 33T/2$. Introducing the total energy U of interaction of the cluster atoms, we have

$$E = U + K\,. \tag{3.4}$$

One can account for the influence of thermal motion of cluster atoms on the parameters of the phase transition on the basis of the anharmonicity parameter η [44, 103, 104], which is introduced for each aggregate state as

$$\eta_{\rm sol} = \frac{K_{\rm sol}}{K_{\rm sol} + U_{\rm sol}}\,, \quad \eta_{\rm liq} = \frac{K_{\rm liq}}{K_{\rm liq} + U_{\rm liq}}\,, \tag{3.5}$$

where each subscript indicates the aggregate state to which it corresponds.

If the atomic motion is that of harmonic oscillators, one has $\eta = 1/2$. Figure 9 gives values of the anharmonicity parameter for the 13-atom Lennard-Jones cluster, which follow from the results of molecular dynamics simulations of an isolated [98] and isothermal [102] cluster. One can see that the liquid state exhibits lower anharmonicity than the solid state because of its looser distribution of atoms. Hence, though the vibrational and configurational degrees of freedom are separable [10] for nearly harmonic motion, due to this change in anharmonicity, parameters of the phase transition depend on the temperature. In particular, Fig. 10 displays the temperature dependence for the entropy jump of the 13-atom Lennard-Jones cluster, which follows from the molecular dynamics simulations [98, 102]. Thus, the entropy jump at the phase transition increases monotonically with an increasing temperature. Using the parameters of formula (3.2) at the melting point, we find the melting point of this cluster [44]:

$$T_{\rm m} \approx 0.3D\,. \tag{3.6}$$

This melting point corresponds to both the isolated and isothermal clusters and also follows from a direct comparison of populations for the solid and liquid aggregate states. From comparison of formulas (3.3) and (3.6) it follows that using the cluster parameters for zero temperature in formula (3.3) would result in doubling the predicted melting point. Ignoring the anharmonicity in treating vibrations as harmonic oscillations leads to a simple version of the solid–liquid phase transitions in clusters [107] that ignores the influence of the thermal motion of atoms on the phase transition.

From an analysis of the 13-atom cluster, one can make general conclusions about the character of configurational and phase transitions in clusters in which interactions between nearest neighbors dominate. The PES of this cluster is characterized by a large number of local minima, more than a thousand [2, 3, 8, 9]. The number of local minima of a PES increases sharply with cluster growth [9]; a cluster's evolution is associated with transitions between local minima of its PES [9, 108]. The thermal motion of the cluster's atoms influences the parameters describing these transitions. Clusters of other sizes behave in the same way. In particular, the Lennard-Jones cluster of 55 atoms is also a closed-shell icosahedron in its ground (solid) state; it has a central atom and two filled, closed icosahedral shells. This cluster and others of a similar size exhibit three aggregate states [100, 109]: solid, liquid, and a state with a solid core and a liquid external shell.

Computer simulations of a 55-atom Lennard-Jones cluster [100, 109–115] allows one to determine parameters of the phase transition from the solid to liquid aggregate state. On the basis of these simulations [44, 103], the cluster's

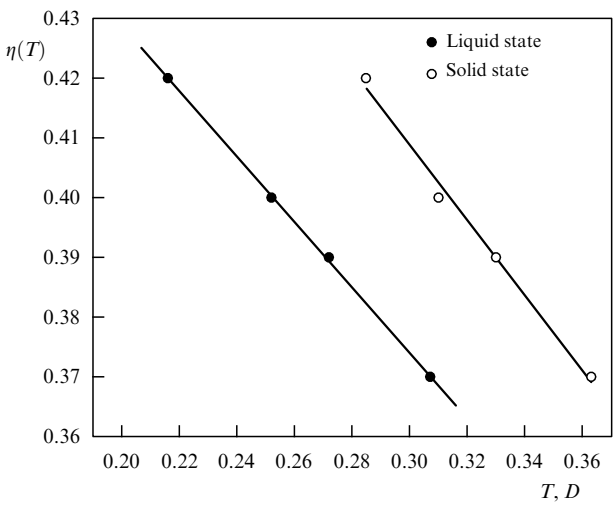

Figure 9. Anharmonicity parameter for a 13-atom Lennard-Jones cluster [105].

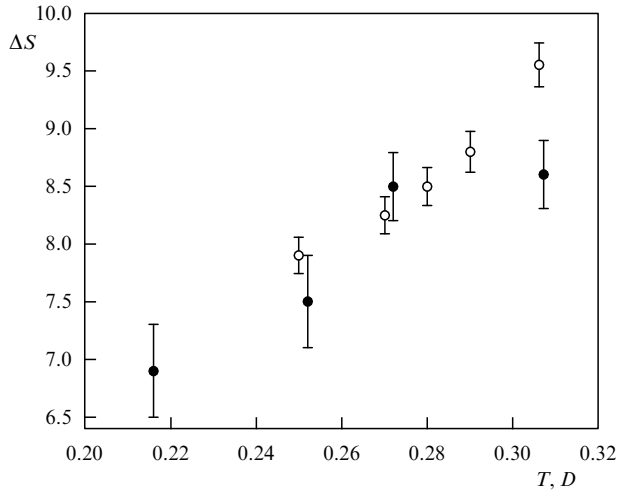

Figure 10. Entropy jump for the phase transition of an isothermal 13-atom Lennard-Jones cluster [106] resulting from molecular dynamics simulations of an isolated [98] and isothermal [102] cluster.

internal energy change is $\Delta E = 15 \pm 1$ at the melting point $T_m = 0.31 \pm 0.01$, and the entropy jump at the phase transition is $\Delta S_0 = 31 \pm 2$ at zero temperature, and $\Delta S_m = 45 \pm 2$ at the melting point. As with smaller clusters, atomic thermal motion increases the entropy jump.

3.3 Interactions in metal clusters

One can expect that the additional low-lying (electronic) degrees of freedom in metal clusters must make them more complex than their dielectric counterparts. But at low temperatures, obviously, electrons in clusters occupy the lower part of the spectrum, and if electronic degrees of freedom are separable from the others, configurational transitions become identical for dielectric and metal clusters. Nevertheless, the specifics of metal clusters are linked to the important role of exchange interactions of bound electrons and to whatever small energy gap the cluster has for configurational excitation. That is, with some low-lying electronic excitations, the system may take on a new, stable geometry different from that of the electronic ground state. The higher the number density of electrons, the stronger the exchange interaction for electrons. Using this, within the framework of a simple model for the potential energy at a given point in the multidimensional space of the PES [116], we have

$$U = \sum_{i,k} V(r_{ik}) - a\sqrt{N_e(\mathbf{r}_i)}\,, \tag{3.7}$$

where $\mathbf{r}_i$ is the set of coordinates of this space point, r_{ik} is the distance between atomic cores i and k, $V(r_{ik})$ is the interaction potential between two atomic cores, a is a numerical coefficient, and $N_e(\mathbf{r}_i)$ is the electron number density at this point. Thus, in this model, we have a pairwise interaction in clusters that leads to the analogy between interactions in dielectric and metal clusters. In particular, for the Sutton–Chen model, the potential energy has the form [117]

$$U = D\left[\sum_{i\neq k}\left(\frac{R_e}{r_{ik}}\right)^n - C\sum_{i\neq k}\left(\frac{R_e}{r_{ik}}\right)^m\right]. \tag{3.8}$$

Table 2 contains the parameters of this interaction potential for the bulk metals which we consider below.

There are various models for interaction within metal clusters (see, for example, Refs [120–126]), which use different forms for the effective interaction potential in the metals. The numerical parameters of these models are chosen so that some of them fit the measured values of the corresponding bulk metals. This procedure is intended to establish the reliability of the values. One of these models uses the Gupta form for the potential [16] together with the parameters of interaction between bound metal atoms in the bulk metal; sometimes, modifications of the Gupta potential are utilized [17, 19]. The tight-binding scheme [14] contains a short-range repulsive interaction potential of atomic cores and exchange interaction of electrons and atomic cores [15, 18]; this creates an energy band in the electronic spectrum. There are also various modifications of the tight-binding scheme [20, 127–131]. The embedded atom method (EAM) based on the Voter–Chen approach is given in papers [132–134].

Table 2. Parameters of the effective interaction potential of atoms in formula (3.8) for bulk metals [118, 119].

	n	m	D, meV	C	R_e, Å
Ni	9	6	16	39	3.52
Ag	12	6	2.5	144	4.09
Au	10	8	13	34	4.08

Density functional theory (DFT) is a more consistent method for modeling clusters. The form of DFT is analogous to that of the Hartree–Fock approximation in which one uses a one-electron approach that yields a self-consistent field acting on a test electron from other electrons and the atomic core. However, instead of wave functions, DFT operates with functionals, specifically density functionals. The variational principle included in DFT [21] allows one to choose the optimal functional among those considered. Therefore, DFT in its standard form describes the ground electronic state of an atomic system. One can expect in the future that DFT will be the leading method in modeling atomic systems because of its consistency and validity. But applying this method for real atomic systems now involves some mathematical problems. This makes simple models more attractive for the present.

At this time, the predictions of configurational states for metal clusters frequently depend on the method used, even for the ground state. Especially, this takes place so for gold clusters because of the small energy gap between the ground and lowest excited configurational states. It appears that interactions within a cluster are determined by valence electrons for which relativistic effects are not essential, even for clusters of heavy atoms. Nevertheless, relativistic effects in inner cores influence cluster energy parameters as a result of compression of the 6s orbital. Accounting for relativistic effects is a complicated problem [135] and they are usually analyzed in clusters in the Pauli approximation if relativistic effects are weak [136, 137]. The analysis of relativistic effects in clusters of heavy elements [138–140] shows that their basic action results from penetration of s-electrons into a region of small distances from the nucleus where the effective charge is significant. In addition to compression of inner shells, this leads to compression of the distribution of valence s-electrons which, in the case of gold, is about 20%. Although relativistic effects only slightly influence the crystal lattice constant which, for gold, decreases less than 10% [141], other cluster parameters may change more due to relativistic effects. In particular, the cohesive energy increases in bulk gold by one and a half times the value in nonrelativistic approximation [141].

Relativistic effects in a gold cluster hamper its computer modeling. In particular, let us consider the gold cluster Au_{13}, since 13 is the lowest magic number for the icosahedral structure, and many other 13-atom metal clusters have an icosahedral structure in their ground configurational state [142], while the structure of the Au_{13} cluster remains a matter of discussion. The icosahedral structure corresponds to the global minimum of the PES according to evaluations [127, 143–146], whereas the icosahedral structure, according to calculations [147, 148], corresponds to an excited configurational state.

Experimental methods give important information for interparticle interactions in metal clusters. The simplest experimental method to determine cluster structure is based on measurements of the cluster mobility. The accuracy of the mobility measurement is approximately 1%, whereas the mobility difference for clusters with the compact and plane

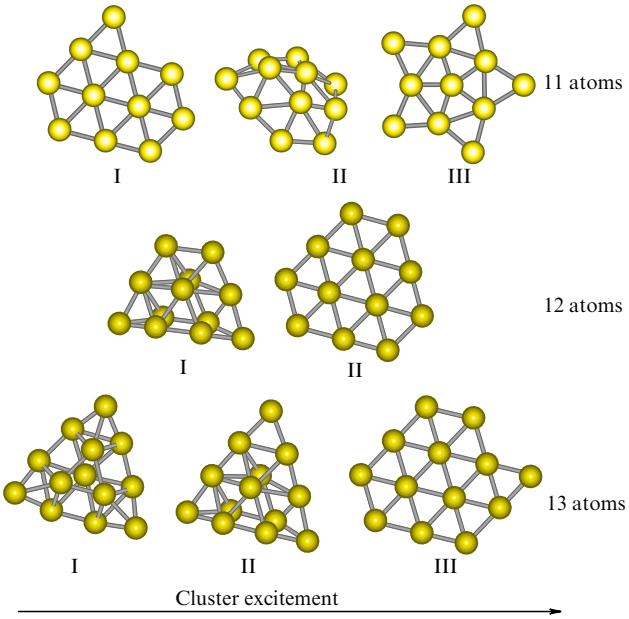

Figure 11. Configurations of lower-energy states of negatively charged gold clusters consisting of 11, 12, and 13 atoms (from left to right as a cluster is excited), according to mobility measurements [149].

structures exceeds 10%. Therefore, measurement of the cluster mobilities in helium at different helium temperatures and their comparison with the calculated mobilities give both an optimal cluster structure at a given temperature and the energetic parameters for transition to another structure. As a demonstration, Fig. 11 demonstrates the sequence of structures for negatively charged gold clusters. Combining these measurements with evaluations [150, 151] shows that the negatively charged cluster Au_{11}^- has a planar structure, in contrast to three-dimensional structures for clusters Au_{12}^- and Au_{13}^-. The transition from the planar structure to the three-dimensional one occurs for negatively charged gold clusters Au_n^- at $n = 12$ [152], while for positive charged clusters Au_n^+, this transition takes place at $n = 7$ [153]. This also demonstrates that the charge of a metal cluster influences its structure.

The electron diffraction method allows us to determine cluster structures from the patterns of electron scattering by free clusters. In particular, this method was applied to determine the structures of negatively charged clusters Au_n^- with $n = 11 - 24$ [154]. Infrared (IR) molecular beam spectroscopy has also been used to study clusters (see, for example, Refs [155–157]), and allows one to determine the cluster distribution in beams. Let us demonstrate the possibilities of this method taking advantage of measurements [157] of IR absorption for neutral gold clusters Au_n, $n = 7 - 20$ in size, in the spectral range $47 - 220$ cm^{-1}. A typical width of absorption lines is about 4 cm^{-1}, while the linewidth of the source of IR radiation is equal approximately to 2 cm^{-1}. The comparison of measured absorption spectra with calculated ones allows us to determine the cluster structure for lower configurational states.

High-resolution photoelectron spectroscopy allows one to determine absorption spectra in the ultraviolet (UV) range (see, for example, Refs [158–165]) for clusters of tens of atoms. These spectra are determined by electronic bound–free transitions as a result of excitation of valence electrons. They consist of some resonant spectral lines which are broadened by the interaction of valence electrons with an environment. Such spectra depend on the cluster structure.

Note that, because of the complex character of the above methods and problems in their interpretation, contemporary experimental methods for studying clusters are frequently combined with computer methods for analyzing the results. In addition, specific experimental methods [166–168] are used for metal clusters.

3.4 Phase transitions in metal clusters

As evidenced by the foregoing, if we neglect energy changes in a cluster due to electronic degrees of freedom and invoke the separation of the electronic and other degrees of freedom, the character of the solid–liquid phase transition in a metal cluster becomes identical to that in a dielectric cluster. Note, however, that there is a big difference between the energies per atom of the configurational excitation for a bulk inert gas with pairwise interactions between atoms and a bulk metal. In particular, the ratio of the melting enthalpy of these systems per atom, $\Delta H_{\rm fus}$, to the atomic binding energy ε_0 in this system is approximately 0.04 for the metals Ni, Cu, Ag, and Au, and 0.2 for argon. This fact leads to a different character of the phase transition for the metal and dielectric bulk atomic systems.

It is convenient to use the model of two aggregate states for the phase transitions of clusters with interatomic pairwise interactions [97, 169–172], where the liquid aggregate state includes a number of configurational states with similar excitation energies. This means that, in the case of clusters with pairwise interaction of atoms, the liquid aggregate state consists of one or several configurational states with similar excitation energies. In the case of metal clusters, the number of configurational states forming the liquid typically varies considerably with the temperature. The difference in the characters of the metal and dielectric phase transitions is demonstrated in Fig. 12, which compares clusters with a pairwise atomic interaction and metal clusters.

In the analysis of the phase transition in metal clusters, we use the results of computer simulations of some 13-atom metal clusters [119, 126, 173, 174] with the Sutton–Chen interaction potential [18] in the cluster. The method of molecular dynamics allows one to take into account the thermal motion of atoms. In contrast to Lennard-Jones clusters [98, 102], in this case, because of the small energy gap between the ground and lowest excited configurational states, it is impossible to determine separately the parameters of the solid and liquid states due to large fluctuations. From this it follows that computer simulation of metal clusters gives less information about their aggregate states than it does for dielectric clusters with interatomic pair interactions.

Let us construct the model of the phase transition for metal clusters, in which, together with thermal atomic motion, we include an additional configurational excitation. Let us represent the entropy jump ΔS near the melting point in the form

$$\Delta S = \Delta S_0 + \Delta S_{\rm t} + \Delta S_{\rm c}\,, \tag{3.9}$$

where ΔS_0 is the entropy jump at zero temperature, $\Delta S_{\rm t}$ is the contribution of thermal motion to the entropy jump, and $\Delta S_{\rm c}$ is the additional entropy due to accessible configurational states. According to the definition, the melting point $T_{\rm m}$ is

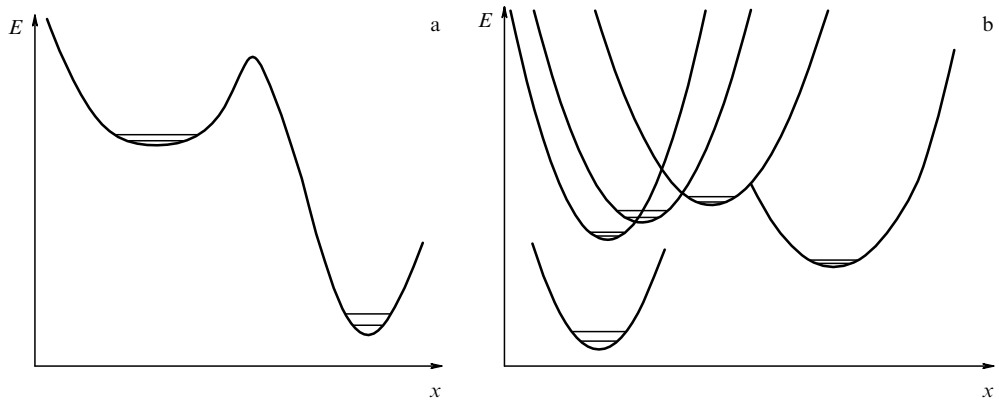

Figure 12. Character of configurational excitation in a dielectric cluster (a) with one excited configurational state of a certain symmetry, and for a metal cluster (b) with a large number of isomers, i.e. with a large number of excited configurational states of similar excitation energies. The coordinate x in the multidimensional atomic space joins the global PES minimum with the indicated local minimum of the PES.

given by

$$\Delta S_{\mathrm{m}} = \frac{\Delta E(T_{\mathrm{m}})}{T_{\mathrm{m}}}\,, \tag{3.10}$$

where ΔS_{m} is the jump of the total entropy at the melting point, and $\Delta E(T_{\mathrm{m}})$ is the change in the configuration energy at the melting point.

In accordance with formula (3.1), the ratio between probabilities of cluster liquid and solid states is given by

$$p(T) = \int \exp\left(-\frac{\Delta E}{T}\right) g(T)\,\mathrm{d}n\,, \tag{3.11}$$

where ΔE is the excitation energy for a given configurational state, $n(E)$ is the number of configurational states with the excitation energy below E, and the factor $g(T)$ characterizes the ratio of statistical weights of the liquid and solid states due to the thermal motion of atoms, where $g(0) = 1$.

Let us represent the dependence of the energy of configurational excitation $\Delta E(n)$ on the isomer number n, the number of configurational excitations with excitation energy below $\Delta E(n)$, as

$$\Delta E(n) = \varDelta_0 + \varDelta_1 \left(\frac{n}{n_0}\right)^{\alpha}. \tag{3.12}$$

This dependence involves three parameters and is represented in Fig. 13 for clusters Ni_{13}, Ag_{13}, Au_{13}. In addition, Table 3 contains parameters of this formula for the indicated clusters, where E_{b} is the total binding energy of atoms in these clusters at zero temperature. The melting points T_{m} of clusters in Table 3 follow from the temperature dependence of the correlation function [47, 48, 98, 99] for the fractional fluctuation of the mean square distance between cluster atoms; this has a sharp jump at the melting point, typically from 0.1 or below to about 0.2. In addition, according to the melting point definition one has $p(T_{\mathrm{m}}) = 1$.

Evaluating integral (3.11) with dependence (3.12) for the energy of cluster excitation, we obtain

$$p(T) = \frac{g(T)}{\alpha} \exp\left(-\frac{\varDelta_0}{T}\right) \left(\frac{n_0 T}{\varDelta_1}\right)^{1/\alpha} \Gamma\left(\frac{1}{\alpha}\right). \tag{3.13}$$

The relation $p(T_{\mathrm{m}}) = 1$ then gives

$$g(T_{\mathrm{m}}) = \alpha \left(\frac{\varDelta_1}{n_0 T_{\mathrm{m}}}\right)^{1/\alpha} \exp\left(\frac{\varDelta_0}{T_{\mathrm{m}}}\right) \Gamma^{-1}\left(\frac{1}{\alpha}\right), \tag{3.14}$$

and from this we find a contribution to the entropy jump $\Delta S_{\mathrm{t}}(T_{\mathrm{m}}) = \ln g(T_{\mathrm{m}})$ which comes from the thermal motion of atoms. Table 3 contains the values of $\Delta S_{\mathrm{t}}(T_{\mathrm{m}})$ for the clusters under consideration here.

The energy change ΔE at the phase transition is the sum of the energy gap $\varDelta_0$ between the ground state and lowest configurational excited state and the energy of configurational excitation within the liquid aggregate state. On the basis of approximation formula (3.12), we have for the energy change:

$$\Delta E = \int E(n)\,\mathrm{d}n$$
$$= \varDelta_0 + \int \exp\left(-\frac{E(n)}{T}\right) g(T)\,E(n)\,\mathrm{d}n = \varDelta_0 + \frac{Tp(T)}{\alpha}\,,$$

Table 3. Parameters of melting of 13-atom metal clusters for $n_0 = 100$.

Parameter \ Cluster	Ni_{13}	Ag_{13}	Au_{13}
E_{b}, eV	44.11	27.87	41.96
$\varDelta_0$, eV	0.73	0.66	0.13
$\varDelta_0/E_{\mathrm{b}}$, %	1.6	2.4	0.31
$\varDelta_1$, eV	0.50	0.42	0.28
α	0.68	0.55	0.58
T_{m}, K	860	820	230
$\Delta E(T_{\mathrm{m}})$, eV	0.84	0.79	0.18
$g(T_{\mathrm{m}})$	280	40	40
δT_{m}, K	200	200	70
$\bar{n}$	13	13	4
ΔS_{t}	5.6	3.7	3.7
ΔS_{m}	11.2	11.3	9.3
$\Delta S_{\mathrm{t}}/\Delta S_{\mathrm{m}}$, %	50	33	40

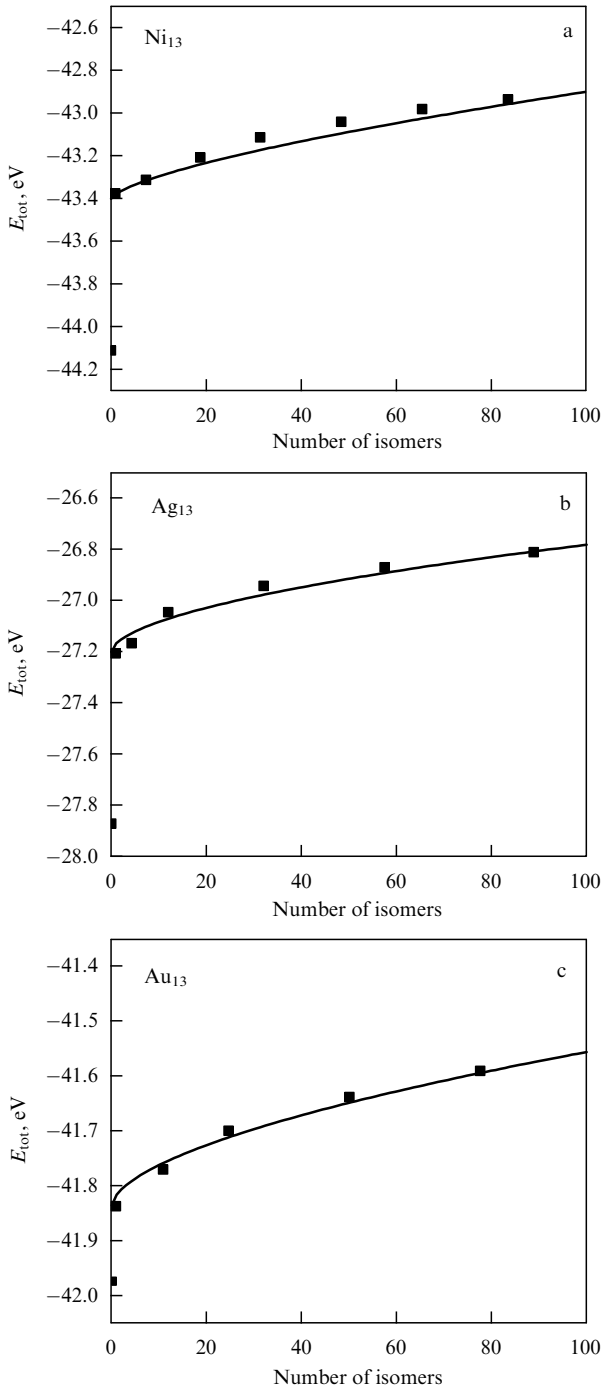

Figure 13. Number of isomers with the excitation energy below an indicated value for metal clusters: (a) Ni_{13}, (b) Ag_{13}, and (c) Au_{13} [119].

and at the melting point this quantity takes the value of

$$\Delta E(T_m) = \Delta_0 + \frac{T_m}{\alpha} . \tag{3.15}$$

Substituting this energy change at the melting point into formula (3.10), we can find the entropy jump ΔS_m at the melting point T_m; its values are given in Table 3. In addition, a further contribution to the entropy jump due to the thermal motion of atoms, $\Delta S_t(T_m)/\Delta S_m$, is also presented in Table 3, thus exhibiting the essential role of atomic vibrations in the phase transitions of metal clusters.

Let us analyze one more aspect of the metal cluster behavior at melting, which is connected with the coexistence of phases. For definiteness, we assume that coexistence of phases is observable in the range [105]

$$0.1 < p(T) < 10 . \tag{3.16}$$

According to formula (3.13), the basic temperature dependence for the ratio between populations $p(T)$ of the liquid and solid states has the form $p(T) \sim \exp(-\Delta E/T)$, which gives the following expression for the width of the observable coexistence range (3.16) of the solid and liquid phases:

$$\delta T_m = \frac{T_m^2 \ln 10}{\Delta E} , \tag{3.17}$$

i.e., we assume $\delta T_m \ll T_m$, and the solid and liquid phases coexist in observable quantities within the temperature range from $T_m - \delta T_m$ up to $T_m + \delta T_m$. Table 3 contains the temperature range δT_m for phase coexistence. We see that phase coexistence for 13-atom metal clusters is observable within a relatively wide range of temperatures.

In evaluating integral (3.11), we use the assumption that the phase transition is determined by many configurational states which form the liquid aggregate state, so that we have a continuous dependence $\Delta E(n)$. The average number of isomers partaking in the phase transition is given by

$$\overline{n} = n_0 \left(\frac{T_m}{\Delta_1} \right)^{1/\alpha} \frac{\Gamma(2/\alpha)}{\Gamma(1/\alpha)} ,$$

and Table 3 contains values of this parameter which justify the approach used. In contrast, the liquid aggregate state of a cluster of atoms with pairwise interactions first involves only one small set of excited configurational states, which is separated from other, higher-excited configurational states by a wide energy gap. Hence, the phase transition in such clusters may be described by the model of two configurational states [104, 171, 172]. On the contrary, the liquid aggregate state of metal clusters includes many configurational states whose number increases even with relatively small increases in cluster excitation.

Let us analyze the reliability of the Table 3 data based on the Sutton–Chen potential [117] as a model potential for atomic interactions in a metal cluster. Comparison for 13-atom metal clusters with the results of other models shows that the cluster structure coincides in the nickel and silver cases, whereas calculations [127, 143–148] for gold clusters with various models do not give the same sequences of cluster structures. This sequence of configurational states of a 13-atom gold cluster according to calculations [119], which we used above, differs from that derived from measurements of the cluster mobility presented in Fig. 11 [149]. Moreover, using the melting point of the 13-atom gold cluster and the density of the energy of configurationally excited states according to calculations [119] leads to contradictions. In order to overcome these latter, we reject the melting point of 430 K found from computer simulations for Au_{13} [119]. Taking the excitation energy $\Delta_0 = 0.15$ eV from these simulations for the lowest configurational state, we determine the melting point such that the contribution of thermal atomic motion to the entropy jump would be 40%. This gives $T_m = 230$ K and is used in Table 3. This fact

testifies to the qualitative character of the Table 3 data for the gold cluster.

To demonstrate the phase transitions in clusters, we used 13-atom clusters as guides. These clusters are convenient for modeling because of their small size and because the liquid state is separated from the solid one by an energy gap, since the outer atomic shell of the solid is complete, with an icosahedral structure. For clusters of a neighboring size, the energy separation is not so great. In particular, computer simulation does not reveal the liquid state of Lennard-Jones clusters consisting of 8 and 14 atoms [175]. Additionally, clusters consisting of 13 atoms are convenient for simulation because they have two clearly distinct aggregate states and, because of particle exchanges, all the atoms of the surface shell partake in the phase transition. This analysis gives a useful insight into the cluster phase transition [176], and, in particular, the role of thermal motion's influence on the parameters of the phase transition for various types of atomic interactions within the cluster.

Let us consider in conclusion the cluster phase transition from another standpoint, on the basis of the possibility of its modeling by contemporary computer methods. Since the solid and liquid aggregate states of a cluster with pairwise atomic interactions are determined by their different atomic configurations, the PES for aggregate cluster states may be found with DFT, which is based on the variational principle and, hence, is valid for the ground electronic state. But since DFT gives cluster parameters at zero temperature and we now know that thermal atomic motion is important for the phase transition, it is useful to combine DFT with molecular dynamics approach. This combination suggested by Car and Parrinello [42] is an essential step in modeling bulk atomic systems, that allows one to calculate their phonon spectra.

4. Catalytic processes involving clusters

4.1 Character of the catalytic process

Catalytic processes have been used in chemistry for at least two centuries. They accelerate a chemical reaction through the action of a catalyst, a substance that is not expended in the chemical process. In heterogeneous catalysis [177–182], the interaction of reacting molecules with the catalyst's surface typically decreases the activation energy (2.2) of the chemical process. But the catalyst's action may involve not only an acceleration of the process, but the introduction of a change to the reaction's pathway [183, 184]. We shall consider physical aspects of the catalytic process, focusing on clusters as catalysts. Such catalytic processes proceed on the cluster surface and are simpler to interpret than a catalytic process involving new chemical pathways.

Note that a requirement for a catalytic process is that a reactant molecule somehow engage a catalytic surface, rather than one in which the reactant molecule directly engages a noncatalytic substrate. For this reason, dielectrics with large energy gaps between their ground and lowest excited states are not suitable as catalysts. On the contrary, metals with a low excitation energy are fitted for this goal. Evidently, a metal surface or metal clusters may be catalysts if the excitation energy for lower configurational states is low enough, so that the local minima of the PES for the lowest excited configurational states are close to the global minimum of the PES. The energetic proximity of excited configurational states of the liquid state of a metal cluster is also sometimes important for this process. Transitions between configurational states of the total system consisting of the metal cluster and an attached reactant molecule can lead to high efficiency of the chemical process through a decrease in the activation energy E_a of the process. In this respect, the cluster works as a catalyst, i.e. it provides a pathway with a higher rate than the uncatalyzed rate without the cluster participation.

This possibility is realized for metal clusters and bulk metals as well, particularly for the surfaces of bulk systems. Hence, metal surfaces are used widely as catalysts [185–187]. At present, metals, as well as metal oxides and metal sulfides, are used as catalysts in the synthesis of inorganic compounds, in cleaning and processing petroleum, and for a wide variety of similar chemical process such as hydrogenation of chemical compounds and the oxidation and decay of nitrogen oxides in reactions with hydrocarbons. Metals are used as catalysts in the form of small particles fastened to stable metal oxides, such as Al_2O_3 or SiO_2. A majority of metals that perform as catalysts fall under group 8 of the Periodic Table. Atoms of catalytic metals may have 3d outer electron shells (Fe, Co, Ni, Cu), 4d electron shells (Rh, Pd, Ag), or a 5d electron shell (Pt). Such metals as Ru and Ir with their 4d and 5d shells filled are used as catalysts restrictedly. Osmium is excluded from this list because of its toxicity. Although the gold atom has 5d valence electrons, bulk gold is chemically inactive and is traditionally considered a noble metal. In all the cases in which a metal may be a catalyst, there is a competition between the outer d-electron shell and s-electron shell with the next higher value of the principal quantum number, so that electronic transitions between s and d electron shells may provide the catalytic action of these metals.

As a demonstration of a chemical process involving a metal catalyst, we will take into consideration a model reaction

$$\mathrm{NO} + \mathrm{CO} \rightarrow \frac{1}{2}\,\mathrm{N_2} + \mathrm{CO_2}\,, \tag{4.1}$$

with Pd_n clusters as catalysts. This process was studied in experiments [188, 189] with palladium clusters comprising the numbers of atoms n from 4 up to 30. These clusters are fastened to a surface of MgO and occupy only about 0.5% of this surface. In the simplest version describing this catalytic process (4.1), two molecules of NO attach to the cluster surface, and their binding with the surface decreases the binding energy between oxygen and nitrogen atoms in the NO molecules. Collision of a CO molecule with surface-bound NO molecule may lead to the transition of an oxygen atom to a CO molecule, forming a CO_2 molecule, leaving nitrogen atoms on the cluster surface joining to form an N_2 molecule. This process proceeds more effectively than in the gaseous phase.

The catalytic process under consideration proceeds according to the scheme

$$2\mathrm{NO} + \mathrm{Sur} \leftrightarrow \mathrm{ON} - \mathrm{Sur} - \mathrm{NO}\,, \tag{4.2}$$

$$2\mathrm{CO} + \mathrm{ON} - \mathrm{Sur} - \mathrm{NO} \rightarrow 2\mathrm{CO_2} + \mathrm{N} - \mathrm{Sur} - \mathrm{N}\,, \tag{4.3}$$

$$\mathrm{N} - \mathrm{Sur} - \mathrm{N} \rightarrow \mathrm{N_2} + \mathrm{Sur}\,, \tag{4.4}$$

where $A - \mathrm{Sur}$ is the bound state of an atomic particle A resided on the surface, and the scheme of the specific chemical

reaction (4.1) has the form

$$2\mathrm{CO} + \mathrm{NO} - \mathrm{Sur} - \mathrm{NO} \leftrightarrow 2\mathrm{CO_2} + \mathrm{N} - \mathrm{Sur} - \mathrm{N}$$
$$\rightarrow 2\mathrm{CO_2} + \mathrm{N_2} + \mathrm{Sur}\,. \tag{4.5}$$

Let us introduce a number of active centers to which molecules may attach, and assume that equilibrium between free and bound molecules is established rapidly, whereas the chemical process proceeds slowly on the time scale of that attachment process and does not violate this equilibrium. Then the probability f that the NO molecule is bound may be determined by the Langmuir isotherm [190]; this probability is given by the expression

$$f = \frac{[\mathrm{NO}]}{[\mathrm{NO}] + N_0 \exp(-\varepsilon_0/T)}\,, \tag{4.6}$$

where [NO] is the number density of free NO molecules, and ε_0 is the binding energy (chemical potential) for NO molecules and the surface; the parameter N_0 is on the order of the atomic value ($N_0 \sim a_0^{-3}$, where a_0 is the Bohr radius). This probability is normalized such, that at high number densities it tends to unity, and at small number densities, it follows the exponential temperature dependence (2.2). Within the framework of the above scheme, a competition takes place between molecular attachment to and detachment from the surface, and the chemical process. At low temperatures, the rate of the chemical process is low because of the activation character of this reaction, and at high temperatures the probability of molecular attachment to the surface is small. Hence, the temperature dependence for the rate constant of the catalytic process must exhibit a maximum at a certain temperature, in accordance with the Sabatier principle [181], which reflects the competition of the indicated processes [191].

From this it follows that the rate of the chemical process (4.1) is expressed as

$$v = j \exp\left(-\frac{E_\mathrm{a}}{T}\right) fs = \sqrt{\frac{T}{2\pi m_\mathrm{B}}} \exp\left(-\frac{E_\mathrm{a}}{T}\right) fs\,, \tag{4.7}$$

where j is the flux of CO molecules to the surface, T is the temperature expressed in energy units, m is the mass of the CO molecule, E_a is the activation energy for the chemical process, f is the probability that the molecule NO is bonded with the surface, and s is the area of the region near the bonded molecule where the chemical process proceeds. Extracting the temperature dependence for the rate constant of the chemical process, we represent the effective rate constant of the chemical process in the form

$$k = \frac{v}{[\mathrm{CO}]} = \frac{k_0 \exp(-E_\mathrm{a}/T)}{1 + (N_0/[\mathrm{NO}]) \exp(-\varepsilon_0/T)}\,, \tag{4.8}$$

where the effective rate constant k_0 is on the order of the rate constant of elastic intermolecular collisions. Thus, the rate constant of the chemical process k involving bound and free molecules has a maximum in the case of $\varepsilon_0 > E_\mathrm{a}$, and the corresponding temperature T_max that follows from equation $\mathrm{d}k/\mathrm{d}T = 0$ is given by [192]

$$T_\mathrm{max} = \varepsilon_0 \left[\ln\left(\frac{N_0}{[\mathrm{CO}]} \frac{\varepsilon_0 - E_\mathrm{a}}{E_\mathrm{a}}\right)\right]^{-1}. \tag{4.9}$$

Let us use formula (4.9) to treat measurements [189] for process (4.1) with clusters Pd_8 and Pd_{30} as catalysts, as shown in Fig. 14. These results relate to partial pressures $p_\mathrm{CO} = 5 \times 10^{-7}$ mbar and $p_\mathrm{NO} = 1 \times 10^{-4}$ mbar. Curve *1* in Fig. 14 is given by formula (4.8) with parameters $\varepsilon_0 = 0.73$ eV, $E_\mathrm{a} = 0.51$ eV for the Pd_8 cluster, and curve *2* in Fig. 14 is that for the Pd_{30} cluster with parameters $\varepsilon_0 = 0.69$ eV, $E_\mathrm{a} = 0.42$ eV in formula (4.8). Note that process (4.1) with Pd_8 and Pd_{30} clusters as catalysts does not reflect the cluster specifics, because bulk palladium may also be used as a catalyst in this process [193–195]. Nevertheless, this analysis exhibits characteristics of the simple heterogeneous catalytic process.

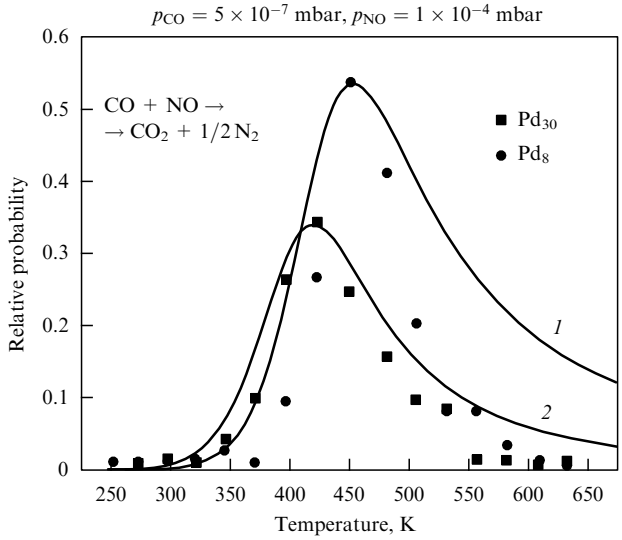

Figure 14. Measured rate constants of process (4.1) with clusters Pd_4 and Pd_{30} as catalysts [188, 189] and the rate constant of this process calculated from formula (4.8) with suitable parameters (solid curves).

4.2 Nanocatalysis

The term 'nanocatalysis' [196–198] refers to processes in which small nanoscale particles act as the catalysts. An example, which we explore in some detail here, involves supported gold clusters consisting of approximately 10 atoms acting as catalysts in processes of oxidation of carbon monoxide and hydrocarbons in an air flow. The variety of oxides that can act as a support for gold clusters as catalysts is rather restricted and includes Fe_2O_3, MgO, TiO_2, and CeO_2 molecules; catalytic effects with other supports are weak. These support compounds may be in the form of micron particles, bulk solids, or films.

It is striking that bulk gold is not a catalyst, whereas small gold clusters are good catalysts for CO oxidation in atmospheric air at room temperature and lower. This effect was discovered by Japanese scientists in 1987 [199–201], who extracted gold clusters and gold particles from a solution of a gold compound and demonstrated that observable catalytic behavior occurs only with particles below 1 nm in size. (The Wigner–Seitz radius [202, 203] of gold is 0.17 nm.) With sizes of gold particles above 5 nm, the catalytic effect disappears altogether. Moreover, the optimal number of gold atoms in a catalytic cluster is now generally accepted as 10 [204–207].

The study of this catalyst and its catalytic effect through both experimental investigations and computer simulations expanded after 2000. These studies have widened our understanding of these clusters and their related processes from

various standpoints, although at present some aspects of these processes remain unclear. It is essential that, at the beginning of the reaction, a supported gold cluster — acting as catalyst — has a bilinear structure; the CO molecule attaches to a cluster boundary to trigger this process, while an oxygen molecule is located on the support surface, where the support is a metal oxide. Next, it is necessary to move some oxygen atoms from the support surface in order to prepare the catalyst. The gold cluster attaches to an oxygen atom and forms a strong chemical bond with it. Note that gold atoms are located above oxygen atoms in the complex structure formed.

Let us consider some applications of this catalyst. Since it provides CO oxidation in atmospheric air at room temperature that is not carried out with other catalysts, it can be utilized in a car filter. The same is true of the oxidation of some hydrocarbons in air with this gold cluster catalyst [208]. Nevertheless, the first application of this catalyst was directed toward smell removal from Japanese toilets [204, 209]. In these catalysts, a zeolite dust with $NiFe_2O_4$ was used as a support. The catalyst provided detachment of trimethylamine, the basic smell source, as a result of trimethylamine decomposition into N_2 and CO_2. The catalysts made of platinum and palladium used for this process at higher temperatures led to the formation of N_2O.

Along with car filters, which could already justify a heightened interest in gold catalysts, these can act as sensors of CO [210] and may be used for the control of CO emission from car motors or for air purification [211]. This nanocatalyst is suitable for use in batteries or as a combustive element with methane [212]. The combustive element transforms the chemical energy as a result of a chemical reaction into electric energy. Notably, oxygen and hydrogen injected in a suitable proportion into the combustion chamber with a platinum combustive element are transformed completely into water vapor. Such an equivalent of combustion creates a voltage of several tenths of a volt. This oxidation process operates in a pulsed regime, and after some time the platinum catalyst becomes blocked. The addition of gold clusters onto the catalyst surface allows one to increase the number of cycles for this process by several times [213, 214].

This catalyst may also find application in so-called green chemistry [215, 216], via the oxidation of a variety of reagents by atmospheric air, forming nitrogen, water, and CO_2. The catalyst under consideration uses gold clusters for such processes [217]. In particular, this catalyst can be utilized for the production of gluconic acid [218], acetic acid [219], and propylene oxides [220]. A nanocatalyst composed of gold clusters provides high efficiency and selectivity for these chemical processes.

One might suppose that there would be a high price for this catalyst, because it contains gold. In reality, the price of nanoparticle gold catalysts is high because of the method of its preparation and its specific requirements, in particular, selectivity for any special cluster size. But this price is determined by the specifics of the apparatus used, and not the price of gold — simply because very little of the metal is required. Indeed, let us calculate the gold price in supported clusters assuming, according to Refs [204, 205, 207, 219], that the optimal number of gold atoms in a supported cluster is 10. We assume the face-centered cubic structure of clusters Au_{10}, i.e. seven atoms form a hexagon in the lower cluster layer and three atoms are located in an upper layer above the hexagon, and also assume that clusters occupy 1% of the support area. Assuming the surface density of gold atoms to be $N_{Au} = 7.8 \times 10^{14}$ cm^{-2} [221], we obtain for the gold mass n_{Au} per surface unit:

$$n_{Au} = 0.01\,\frac{10}{7}\,M\,N_{Au} = 4 \times 10^{-9}\ \text{g cm}^{-2}\,,$$

where M is the mass of a gold atom. Taking the market price of gold to be \$ 1700/ounce, we obtain for the specific gold price of this catalyst 0.3 cents m^{-2}. Thus, the contribution of the catalyst material to its price is small, and the catalyst price is determined both by an elaborate apparatus which allows one to produce nanoobjects with the required parameters and qualified personnel who can work with such an apparatus.

Our task is now to understand the nature and operation mechanisms of the nanocatalysis under consideration. Note that contemporary methods of detection allow one to resolve and even to move individual atoms. The theoretical analysis relates to the dynamics of transitions in a complex atomic system and is based on describing transitions between configurational states and uses an understanding similar to that for configurational transitions in simple atomic systems (see Sections 2, 3). For the simplest atomic systems, a configurational transition corresponds to transitions between electronic terms for a system of colliding atomic particles [222] under conditions in which the relative velocity of the colliding atomic particles is small compared to typical electron velocities. If we pass from simple atomic systems — atomic particles — to complex atomic systems, say, to clusters, this leads to change in the method of the analysis of these processes from electronic terms to the effective surface of internal cluster energy, the PES [9, 108].

4.3 General principles of nanocatalysis

According to this analysis of nanocatalyst behavior, it is necessary for a gold cluster to have different configurations with similar energies. This is appropriate for gold clusters for two reasons. First, the electronic 5d and 6s shells of the gold atom are close in energy, and these shells compete in a system consisting of a gold cluster and a reactant molecule. Second, relativistic interactions affect the contribution of 5d and 6s electron shells of the gold atoms in the chemical binding of gold cluster atoms. We can expect clusters of a given size but with different geometric structures to have different electronic shell populations and, consequently, different bonding characteristics. Of course, those differences will influence the nature of transitions among the various structures during a reaction. Specifically, these electron interactions must influence the configurational transition between the planar bilayer and the three-dimensional structures of gold clusters.

The basic advantage of using gold clusters as catalysts is the possibility to carry out the oxidation process at room temperature and lower, something inaccessible with other catalysts. As a result, this catalyst may be used in some particular applications, a consideration that gives particular interest to this catalyst. We recognize that fundamental interest in this paper, and our goal is to understand conditions which enable proceeding of such a low-temperature chemical process. Therefore, based on the physical aspects of this problem, we concentrate our attention on the simplest chemical process of this type, CO oxidation in atmospheric air, which proceeds according to the scheme

$$2CO + O_2 \rightarrow 2CO_2\,. \tag{4.10}$$

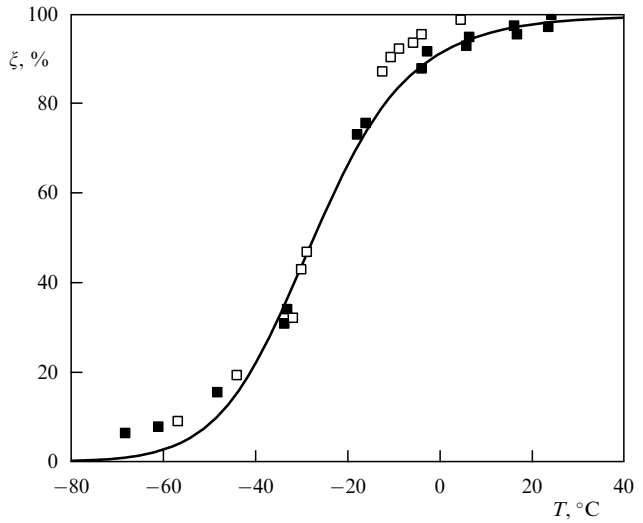

Figure 15. The portion of CO molecules transformed into CO_2 molecules in an air flow with Au/TiO_2 catalysts, as a function of temperature for a standard reactor [204, 224].

Since the binding energy of the system CO – O is 5.45 eV, and the O – O binding energy is 5.12 eV [223], even the chemical reaction involving the bond breaking in the oxygen molecule

$$CO + O_2 \rightarrow CO_2 + O\,, \tag{4.11}$$

proceeds with an energy release of 0.33 eV per molecule. The following stage involving an oxygen atom,

$$CO + O \rightarrow CO_2\,, \tag{4.12}$$

proceeds with the energy release of 5.45 eV, equal to the CO – O binding energy. Hence, the limitation on the rate of the process (4.10) in the gaseous phase is determined by the behavior of electronic terms for this process, rather than its configurational energetics.

As was indicated, the advantage of employing the nanocatalyst of gold clusters on a suitable support surface is a consequence of the low temperature of the chemical process (4.10). This is demonstrated in Fig. 15 [204, 224], which shows the portion ξ of CO molecules transformed into CO_2 under standard conditions in an air flow with an admixture of CO in the chemical reactor (the concentration of CO molecules in air is typically 1%), the gold clusters are located on the surface of TiO_2. The portion ξ of transformed molecules also depends on the reactor parameters, mostly on the residence time of the air sample with admixtures and the total surface area for the catalyst. It is apparent that the conditions of each experiment may be reduced to standard conditions [224]. Next, the quantity ξ also depends on the cluster size, which, in turn, is determined by the method of preparation of the catalyst. Figure 15 contains the results reduced to identical parameters of the chemical process.

Let us treat the results of Fig. 15 within the framework of the model according to which the evolution of the CO molecule attached to a cluster may develop along two completely different channels. One of these corresponds to the formation of the CO_2 molecule. Characterizing the process flow time for these channels by typical times τ_1 and τ_2, we arrive at the probability of CO_2 formation in a given process:

$$P_1 = \frac{\tau_1}{\tau_1 + \tau_2}\,. \tag{4.13}$$

In accordance with the Arrhenius formula (2.2), we obtain the following expressions for these times:

$$\tau_1 = a \exp\left(\frac{\varepsilon_1}{T}\right), \quad \tau_2 = b \exp\left(\frac{\varepsilon_2}{T}\right), \tag{4.14}$$

where ε_1 and ε_2 are the activation energies for these channels, and a and b are constants. Correspondingly, formula (4.13) may be rewritten in the form

$$P_1 = \frac{1}{1 + A \exp\left(E_a/T\right)}\,, \tag{4.15}$$

and its parameters according to the data of Fig. 15 are $E_a = \varepsilon_1 - \varepsilon_2 = 0.50$ eV and $A = b/a = 6.4 \times 10^{-11}$. This value of the activation energy E_a is typical for chemical processes, whereas for such processes $A \sim 1$. A small value of this parameter, in accordance with the experimental data of Fig. 15, testifies to the specifics of the competition of processes. We explain this by a difference in the nature of the two channels for this process [225, 226]: namely, one of these channels corresponds to a change in the electronic structure of the system as a result of a transition which is similar to charge exchange. The other is purely a process of configurational change.

In considering this mechanism for one of the channels of this process, we take into account the electron affinity of free gold clusters consisting of 10–20 atoms, which lies in the range from 3 to 4 eV [227]. The probability of a tunneling transition between two potential wells separated by a distance l is given by [222]

$$P = \exp\left(-\frac{\sqrt{2m_e\varepsilon}\, l}{\hbar}\right), \tag{4.16}$$

where m_e is the electron mass, and ε is the potential barrier height, which corresponds to the well depths or the electron affinities of the structures in the two wells, assumed to be identical. For typical values of the electron binding energy between $\varepsilon = 3$ eV and $\varepsilon = 4$ eV, the distance between wells is $l = 1.6$ nm and $l = 1.1$ nm, respectively, if we use the above rate of the electron transition, $P = 6 \times 10^{-11}$. For comparison, the Wigner–Seitz radius for gold is $r_W = 1.65$ Å [92, 228]. Hence, the distance l for an electron transition exceeds the cluster size, which is approximately 1 nm. From this it follows that the mechanism for the process of releasing the CO molecule involves the passage of an electron from the gold cluster to an oxygen atom that is located on a support.

On the basis of this analysis, we propose the following scheme of the catalytic process of interest [226, 229]:

$$CO + \widetilde{Au_n} \rightarrow CO - \widetilde{Au_n}\,, \tag{4.17}$$

$$\widetilde{O} + CO - \widetilde{Au_n} \rightarrow CO_2 - \widetilde{Au_n} \rightarrow CO_2^- + \widetilde{Au_n^+}\,, \tag{4.18}$$

$$\widetilde{O^-} + CO - \widetilde{Au_n} \rightarrow \widetilde{O} + CO - \widetilde{Au_n^-}\,, \tag{4.19}$$

where $CO - \widetilde{Au_n}$ is the bound state of the indicated particles. The second and third competing processes, (4.18) and (4.19), include stable states of the complex atomic system, and they depend on the point where an oxygen atom attaches to a united CO – gold cluster system, and the latter may be either neutral or negatively charged. Of course, a cluster can capture

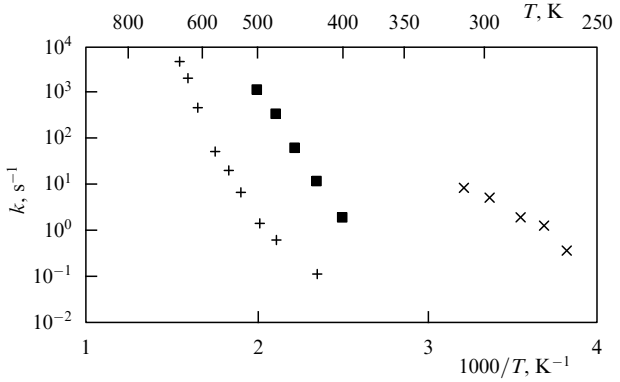

Figure 16. Temperature dependence of the rate constant for CO oxidation in an air flow in a standard reactor [204], which gives the following activation energies E_a for process (4.10): (+) Pt(100), $E_a = 120$ kJ mol^{-1}, (■) Ru(001), $E_a = 120$ kJ mol^{-1}, and (×) Au/TiO_2, $E_a = 30$ kJ mol^{-1}.

an electron from a support, and this process corresponds to the third process (4.19) on this scheme.

In the notation we have used to describe gold cluster catalysis for the oxidation of CO and other carbon compounds in air at room temperature and lower, we illustrate the unique properties of such a catalyst in Fig. 16. There, the rate constants of the process (4.10) in air are given in a temperature range where these rate constants are approximated by the Arrhenius formula (2.2). One can see that the catalytic action with gold clusters does function at lower temperatures.

The complexity of process (4.10) with a cluster catalyst is determined both by the complex structure of a catalyst consisting of different objects and by the structure of its support, where centers for formation of positive and negative ions are located. Hence, the process of CO oxidation is not only multistage but can also include competing elementary processes for transitions between certain configurational states. This is demonstrated in Fig. 17, where the rate constant of CO oxidation in an air flow with the Au/TiO_2 catalyst is given for a wide temperature range, and for different elementary processes proceeding within a general scheme (4.10), each with its own activation energy (2.2). Each process can dominate in a corresponding temperature range. One more demonstration of the complexity of the process (4.10) is given in Fig. 18 [231, 232]. The unit of the layer depth 1 ML in this figure corresponds to support covering by one monolayer of oxygen molecules.

The complexity of the catalyst under consideration is also connected with the dependence of its parameters on the support, its chemical composition, and the state and direction of the crystal lattice of its surface. The simplest version of the support structure to interpret is the (111) lattice face of the magnesium oxide (MgO) crystal, although other metal oxides may also be used as the catalyst support, e.g. α-Fe_2O_3 [233–238], TiO_2 [239–245], and CeO_2 [246, 247]. These compounds exhaust the list of suitable identified supports for this nanocatalyst. The support may be in the form of a macroscopic surface, micron-sized particles, or thin films. We see that all the suitable compounds are metal oxides, and oxygen may take part in the chemical process (4.10). These supports are semiconductors, and their chemical binding with gold clusters may lead to cluster charging that we might assume is important for the catalytic process [135, 248–251]. After all, small gold clusters have electron affinities of order 3 eV,

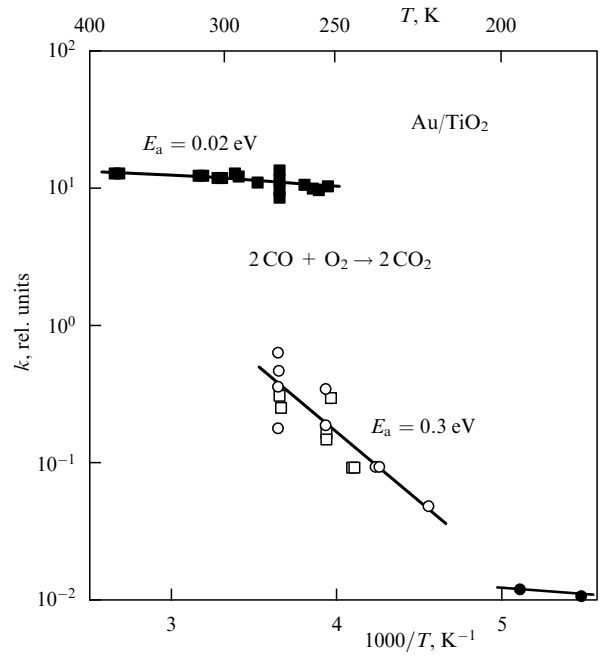

Figure 17. Temperature dependence of the rate constant of CO oxidation in an air flow [process (4.10)] with Au/TiO_2 as the catalyst [230].

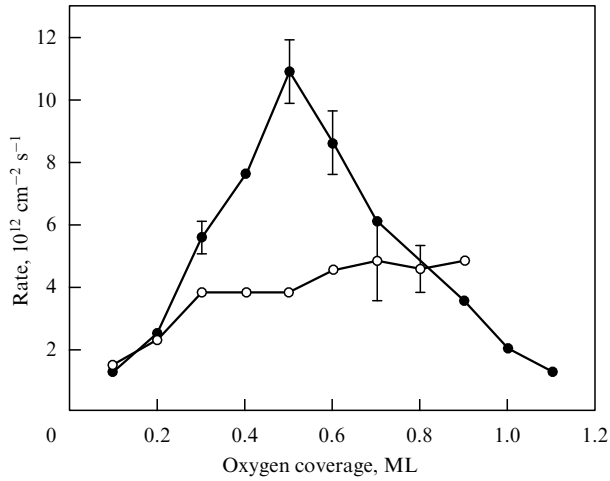

Figure 18. Dependence of the CO_2 formation rate in the process (4.10) on the degree of support covering by molecular oxygen at a temperature of 200 K (filled circles), and 400 K (open circles) [231, 232].

comparable with those of halogen atoms. Note that through this analysis we treat the nanocatalyst as being on a macroscopic support, say MgO, with attached gold clusters, an MgO film consisting of several atomic layers may also be used as a support. This can take the form of a film grown on a macroscopic surface of Mo(100) or Ag(100), with the gold clusters attached to the thin MgO film [252–255]. These investigations exhibit the complexity of this gold cluster catalyst and its sensitivity to the support properties and cluster size.

4.4 Computer modeling of nanocatalysis with gold clusters

Along with experimental investigations, computer modeling is contributing to our understanding of this catalytic process. In spite of the limited accuracy and reliability of individual

computer simulations, the totality of appropriate calculations is helping to reveal properties of the atomic gold cluster system, its attached reactant molecules (here CO), and a solid metal oxide support. The simplest version of simulations of this catalyst based on DFT [21, 22] is the local density approximation (LDA) [22], which operates under the assumption that the exchange interaction potential in the atomic system of interest is proportional to the electron number density at every point, and the partial exchange interaction depends only on the total electron number density. This approximation is refined by dividing the electrons into two groups, with opposite spins and introducing separate dependences of the partial exchange interaction on the electron number densities with each spin direction, namely the local spin density approximation (LSDA). In a more advanced version of DFT, the generalized gradient approximation (GGA) [256, 257], the partial exchange interaction at a given point depends both on the electron number densities with each spin direction and on their gradients.

For the last 50 years, after the introduction of DFT [21, 22], this method has yielded a wide variety of packets of codes. In the simplest versions of this method, the basic functionals are derived from simple plane wave functions. But even in this DFT version, in which the basis is adequate for a uniform spatial distribution of electrons, the self-consistency of the equations' nonuniform potentials leads to a nonuniform spatial distribution of electrons whose number density increases in regions close to nuclei. Hence, self-consistent DFT equations improve a seed distribution of the electron number density. But within the framework of any particular packet of codes, it is impossible to determine the accuracy and reliability of the results.

Nevertheless, because of the absence of an alternative to DFT in computer simulation of complex atomic systems, DFT has been used repeatedly to model nanocatalysis. In particular, such calculations are represented in papers [248, 250, 251, 258–276], enough that a comparison of results of different calculations under identical conditions allows one to improve the reliability of these calculations. The accuracy of such calculations according to Ref. [277] is 1% for the length of chemical bonds, and 25–30% for the heights of the barriers for chemical reactions. But these conclusions still raise doubts because of the model character of DFT, and the accuracy of a model theory cannot be estimated simply by computed numerical results. Fundamentally, we still await a derivation of DFT that shows in a rigorous way how to incorporate the effects of electron exchange and correlation, a way that would enable us to replace the empirical methods currently used to try to describe these effects.

Although the principal properties of a catalyst are determined by the rates of the relevant chemical processes, a contemporary DFT often addresses the less ambitious task of determining stable structures for a complex atomic system. The results of DFT for the geometric distribution of atoms in a complex atomic system appear to be reliable and cannot be obtained by other methods. As a demonstration of DFT's application for this goal, Fig. 19 displays the structures formed by an Au_{10} cluster supported by a solid MgO oxide. Two structures of the gold cluster are possible in this case, the three-dimensional and planar geometries (see Fig. 11). They are characterized by different energy parameters, and the transition between these structures proceeds via the catalytic process.

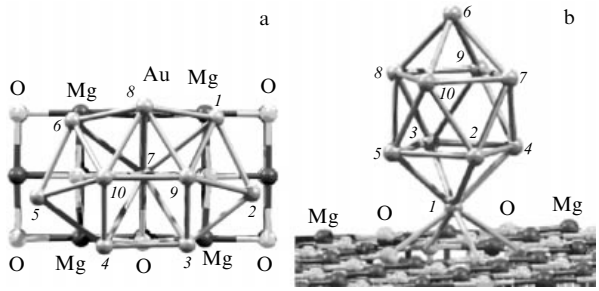

Figure 19. Structures of Au_{10} gold clusters attached to an MgO surface, where gold atoms are numbered [251]. At first, a defect is formed on the {111} surface of the MgO by removal of an oxygen atom from the support, and the lowest gold atom is fastened to this defect.

Let us examine some results of DFT calculations. If a gold cluster with a cubic face-centered structure is located on the surface of MgO, the match of the surfaces Au(100)/MgO(100) is favored, since the constants of the crystal lattice of bulk gold (4.08 Å) and magnesium oxide (4.20 Å) are similar, and these compounds may be in contact with relatively little distortion of parameters of the gold structure. Hence, the Au_{10} cluster with the face-centered cubic structure is a suitable model for the catalyst under consideration [135]. Next, the optimal structure for the combination of the components under consideration corresponds to locating the gold atoms in the combined structure above oxygen atoms of the MgO crystal lattice [274]. Evidently, the structure drawn in Fig. 19a is optimal for this catalyst, while the structure in Fig. 19b corresponds to an excited configurational state of this system. Of course, the description of the static structures, however relevant, gives only a part of the information relevant to the catalytic process.

Thus, DFT is the most appropriate available method for computer simulation of such a complex atomic system, but in its contemporary state, it cannot compete with existing *ab initio* methods for the analysis of simple atomic systems, and, hence, the reliability of DFT for complex atomic systems is problematic. Indeed, model assumptions for the interaction of electrons and ions introduced in the analysis of clusters as simple atomic systems or pseudopotentials and are required for some interactions. This has an analogy with the Kohn–Sham equations [22] in DFT which correspond to the one-electron approximation in the analysis of an atomic system. The next step in modeling large metal clusters may include the application of these models to a bulk metal, which allows one to fit interaction parameters to real systems and provides more reliability of the results. This reliability increases with comparison of the results of more models. As a fine tool, DFT requires careful tuning and high skills of those who use it. In most contemporary computer codes, such tuning capability is absent. Typical contemporary DFT codes do not permit such changes, limiting their applicability to some kinds of systems. For example, contemporary DFT does not allow one to determine the ionization potentials of heavy atoms, the electron affinities of atoms, etc., and, hence, cannot compete with more basic methods for addressing these tasks, whereas the first step in applications of some methods for complex systems is their verification for rather simple systems.

The subsequent development of DFT for the analysis of complex atomic systems will probably lead to a transition from universality to specific applicability for certain atomic systems and to the possibility of modifying computer codes in packets of codes in order to adapt the approach to a specific problem. Of course, there is currently no alternative to DFT for the analysis of complex atomic systems. At present, DFT allows one to construct geometric structures for complex atomic systems, because the distances between nearest neighbors are not sensitive to extended interactions within atomic systems. (An alternative approach based on multi-electron wave functions may have promise in this area [278].)

4.5 Peculiarities of nanocatalysis

The catalytic process includes several subsequent stages which give a unique character to the process. One cannot think simply in terms of the static structures formed at its intermediate stages. Therefore, a certain flexibility in the interpretation of the process is required that can be described by the term 'dynamic fluctuation' [248, 252]. This is connected with effective transitions between configurational states in each intermediate stage, meaning that a system consists of a catalyst and reactant molecule or molecules which undergo effective transitions between initial, intermediate, and final configurational states in this process. Because metal clusters can change their atomic configuration more effectively than can a bulk metal surface, clusters may be more efficient catalysts than macroscopic metal surfaces [279]. This possibility follows for metal clusters because of the typical large number of low-lying excited configurational states [165, 280–282].

Let us examine some experimental results for the catalytic process (4.10) with gold clusters as a catalyst. There is a requirement in this case that boundary cluster atoms be characterized by a low coordination number [187, 204, 282]. For process (4.10), the optimal number of atoms in a gold cluster is 10, whereas for other chemical processes with small gold cluster catalysts the optimal number of cluster atoms may differ (see, for example, Refs [284, 285]). In any case, the gold cluster has two or three atomic layers above the support [286–288]. If the cluster consists of two atomic layers, CO molecules in the chemical process (4.10) attach to the cluster between these layers on the cluster periphery, and oxygen molecules attach to the support [187, 204, 289]. It is possible that oxygen atoms residing in the support also take part in the process of CO oxidation, in which case the infrared absorption of CO molecules may be utilized to detect and identify the location of these molecules. In this case, the absorption spectrum of attached CO molecules is characterized by transition energies of 2112 and 2151 cm^{-1} [290, 291]. Isotope experiments might be used to distinguish the extent to which the oxygen atoms adding to the CO molecules come from the substance or from the attached oxygen molecules.

An indication of the complexity of catalytic chemical process (4.10) is that its rate is not described by the Arrhenius law (2.2) (Fig. 14) which is valid for a typical chemical process. Generalizing the experimental results, we represent the rate constant of process (4.10) in the form

$$v = \mathrm{const}\,[\mathrm{CO}]^{\alpha}[\mathrm{O}_2]^{\beta}\,\exp\left(-\frac{E_{\mathrm{a}}}{T}\right). \qquad (4.20)$$

If we adjust the parameters of an air flow with a CO admixture in the chemical reactor to identical conditions [77, 292], we can obtain the limits, for the $\mathrm{Au/TiO_2}$ catalyst, of the parameters in this formula as follows: $\alpha = 0.05 - 0.85$, $\beta = 0.07 - 0.46$, $E_a = 10 - 30$ kJ mol^{-1} [77], if we use a series of measurements. In particular, for this catalyst at the temperature 273 K, the dependence of the rate of this process on the CO concentration takes the form $v \sim [\mathrm{CO}]^{0.05}$, if the CO concentration varies in air from 0.1 to 10%, and the dependence on the concentration of $\mathrm{O_2}$ molecule follows formulas $v \sim [\mathrm{O_2}]^{0.24}$, if its concentration in air varies from 1% up to 30%. Note that if the catalyst's role reduces to decreasing the activation energy, we would have $\alpha = \beta = 1$ in formula (4.20).

It should be noted that the absorption of CO and $\mathrm{O_2}$ molecules holds true for both a macroscopic gold surface of a terraced shape [135, 232, 293] and a surface of free gold clusters [294, 295]. But process (4.10) proceeds more effectively if the gold cluster is attached to a bulk surface of some metal oxides [201, 283], where attached atoms are located on a cluster periphery and on the boundary between the cluster and support [187, 204]. The bond lengths between cluster atoms vary depending on the surface structure of the support with which the cluster is bonded [219, 286, 296–298]. The character of subsequent attachment of reacting molecules to a cluster depends on the cluster structure. It is usually accepted that contact with a support corresponds to the direction Au(111) of the gold surface [299–301].

Water vapor seems to have some influence on the rate of process (4.10) if the water is in the air flow. This question was investigated in book [77], and its analysis testifies to both the positive and negative influence of water on the rate of process (4.10). Acceleration of chemical processes in the presence of water vapor has been observed for catalysis by gold and other transient elements [171, 302–306]. Two mechanisms have been proposed for water vapor to accelerate process (4.10). According to the first mechanism [307], the catalyst decreases the barrier for dissociation of water molecules which are bonded to the catalyst surface, whereas the second mechanism [297, 308] attributes the effect to the formation of OH radicals or of complexes which contain these radicals. In any case, this effect testifies to the complexity of this catalytic process.

We suppose that in the first stage of the chemical process involving gaseous molecules and supported cluster-catalysts, a reactant molecule attaches to a cluster, an event that changes its structure, and then, in the second stage of the process, the bonded molecule reacts with another reactant. Then, as the last stage of this process, a newly formed molecule releases, while the cluster returns to its initial state [192]. It is clear that the rates of these processes depend on the cluster's charge. A small cluster floating in a gas (including an ionized gas) is most likely neutral with a probability close to unity, but if it is bonded to a support, the cluster may acquire a charge, with its value depending on both the cluster and the support. The cluster charge may be changed also as a result of configurational transitions. In particular, if the $\mathrm{Au_{10}}$ gold cluster is located on the surface of MgO, then according to calculations [251], the total cluster charge reaches $-0.88e$ and $-2.19e$ for different positions of the central atom if the cluster has a face-centered cubic structure (see Fig. 19), but the charge is $-1.06e$ if the cluster consists of two antiprisms.

Summing up the above results for the chemical catalytic process (4.10), within the framework of the PES concept [9], one can formulate a working scheme of this process which includes three configurational states for this atomic system.

In the initial state, a free CO molecule interacts with a gold cluster which is bonded to the macroscopic metal oxide surface according to Fig. 19. The support surface is partially covered by oxygen and is not uniform, but contains active centers (dislocations and admixture atoms), and positive or negative ions are located on these centers. A configurational state resulting from attachment of a CO molecule to a gold cluster is formed with a simultaneous change of the cluster structure (from three-dimensional to planar or vice versa), and an electron transfer occurs to the cluster surface from a nearby negatively charged center. The reverse transition proceeds with simultaneous breaking of the bond between the CO molecule and a gold cluster and with a support. Another configurational state corresponds to the final channel of the chemical reaction, which involves the establishment of a bond between the CO molecule and an oxygen atom located on the support, followed by the release of the CO_2 molecule and transition of the negatively charged gold cluster on the support to another configurational state, in which the gold cluster has a full, 3-dimensional structure. Then, catalytic process (4.10) results from the transitions among these states. Although this scheme is rather complex, it does not contradict our experience or experimental results obtained in studying this process. Notably, this process is realized for a narrow range of cluster sizes and for restricted types of the support.

5. Conclusion

The preceding analysis gives evidence that the nature of various atomic systems may be considered from a common standpoint, based on configurational states of atomic systems. Each configurational state corresponds to a local minimum of the PES, and the evolution of an atomic system involves a chain of transitions between neighboring local minima of the PES [9]. This concept opens up possibilities for computer simulations of complex atomic systems, such as reacting biological structures [108, 309] or nanocatalysis, as analyzed here. One of the questions raised in this paper is how to find ways to understand these possibilities. We can describe the evolution of the motions of an atomic system as classical motion of its atoms in their phase space. Within the framework of this concept, we restrict our description to atomic coordinates, only adding that the system is located at each time in some configurational state, and transitions between configurational states characterize the evolution of this system.

Among computer methods developed for analyzing complex atomic systems, we choose DFT, which is fundamentally able to describe them. As follows from the above analysis, this theory has been applied in recent decades to the complex nanocatalytic systems consisting of gold clusters attached to the surface of a metal oxide. There are many evaluations using this method, and some of those were analyzed here. But it is necessary to accept the results of these evaluations with some caution, because they do not yield good accuracy estimations. Moreover, the capabilities of contemporary DFT are limited. Currently, this theory cannot compete with experimental methods for determining the electron affinities of atoms, for example, and leads to contradictory results for the structure of gold clusters, as discussed above. Moreover, model methods evaluating some properties of metal clusters, including phase transitions, give more reliable results than those of DFT. Hence, the range of application of contemporary DFT is restricted; in particular, DFT is useful for determination of complex cluster structures, an example of which is given in Fig. 19. One can expect the future development of DFT to involve the creation of flexible computer codes within the framework of this method, codes that will focus on evaluation of the PESs for certain atomic systems.

According to the above analysis, the thermal motion of atoms is important for the dynamics of atomic systems at nonzero temperature. In particular, the activation energy for a simple chemical process (2.3) differs from the barrier height for this process and, in the case of the phase transition for a 13-atom Lennard-Jones cluster, neglecting the thermal motion of cluster atoms doubles the predicted cluster melting point. Therefore, computer simulation of complex atomic systems requires joining DFT and molecular dynamics, i.e. combining static and dynamic theories. One can expect progress in the analysis of complex atomic systems, such as physical nanotechnological and molecular biological objects in biophysics, as a result of combination of the above methods.

It should be noted in conclusion, that along with the analysis of physical objects and the phenomena under consideration, the goal of this paper is to formulate and to ground a mathematical method for the analysis of complex atomic systems. The analysis indicates that, when the expected developments are fulfilled, the result will exhibit the perspective position of combining DFT and molecular dynamics for a full understanding of complex chemical reactions.

References

1. Marcelin R *Ann. Physique* **3** 152 (1915)
2. Hoare M R, Pal P *Adv. Phys.* **20** 161 (1971)
3. Hoare M R, Pal P *Adv. Phys.* **24** 645 (1975)
4. Hoare M R *Adv. Chem. Phys.* **40** 49 (1979)
5. Stillinger F H, Weber T A *Phys. Rev. A* **25** 978 (1982)
6. Stillinger F H, Weber T A *Phys. Rev. A* **28** 2408 (1983)
7. Corti D S et al. *Phys. Rev. E* **55** 5522 (1997)
8. Komatsuzaki T, Berry R S *J. Chem. Phys.* **110** 9160 (1999)
9. Wales D J *Energy Landscapes* (Cambridge: Cambridge Univ. Press, 2003)
10. Vekhter B, Ball K D, Rose J, Berry R S *J. Chem. Phys.* **106** 4644 (1997)
11. Jones J E, Ingham A E *Proc. R. Soc. Lond. A* **107** 636 (1925)
12. Jones J E *Proc. R. Soc. Lond. A* **106** 463 (1924)
13. Smirnov B M *Principles of Statistical Physics* (Weinheim: Wiley-VCH, 2006)
14. Friedel J, in *Physics of Metals* Vol. 1 *Electrons* (Ed. J M Ziman) (London: Cambridge Univ. Press, 1969)
15. Chadi D J *Phys. Rev. B* **19** 2074 (1979)
16. Gupta R P *Phys. Rev. B* **23** 6265 (1981)
17. Tománek D, Mukherjee S, Bennemann K H *Phys. Rev. B* **28** 665 (1983)
18. Sutton A P et al. *J. Phys. C Solid State Phys.* **21** 35 (1988)
19. Sawada S, Sugano S *Z. Phys. D* **14** 247 (1989)
20. Cleri F, Rosato V *Phys. Rev. B* **48** 22 (1993)
21. Hohenberg P, Kohn W *Phys. Rev.* **136** B864 (1964)
22. Kohn W, Sham L J *Phys. Rev.* **140** A1133 (1965)
23. Parr R G, Yang W *Density-Functional Theory of Atoms and Molecules* (New York: Oxford Univ. Press, 1989)
24. Dreizler R M, Gross E K U *Density Functional Theory: An Approach to the Quantum Many-Body Problem* (Berlin: Springer-Verlag, 1990)
25. Koch W, Holthausen M C *A Chemist's Guide to Density Functional Theory* (Weinheim: Wiley-VCH, 2000)
26. Fiolhais C, Nogueira F, Marques M (Eds) *A Primer in Density Functional Theory* (Berlin: Springer, 2003)

27. Sholl D S, Steckel J A *Density Functional Theory: A Practical Introduction* (Hoboken, N.J.: Wiley, 2009)
28. Burke K *J. Chem. Phys.* **136** 150901 (2012)
29. Alder B J, Wainwright T E *J. Chem. Phys.* **27** 1208 (1957)
30. Alder B J, Wainwright T E *J. Chem. Phys.* **31** 459 (1959)
31. Rahman A *Phys. Rev.* **136** A405 (1964)
32. Stillinger F H, Rahman A *J. Chem. Phys.* **60** 1545 (1974)
33. Haile J M *Molecular Dynamics Simulation: Elementary Methods* (New York: Wiley, 1992)
34. Rapaport D C *The Art of Molecular Dynamics Simulation* (Cambridge: Cambridge Univ. Press, 1995)
35. Leach A R *Molecular Modelling: Principles and Applications* (New York: Wiley, 1992)
36. Schlick T *Molecular Modelling and Simulation: An Interdisciplinary Guide* (New York: Springer, 2002)
37. Griebel M, Knapek S, Zumbusch G *Numerical Simulation in Molecular Dynamics* (Berlin: Springer, 2007)
38. Hypercube, Inc., http://www.hyper.com/
39. University of Illinois at Urbana-Champaign. Theoretical and Computational Biophysics Group. Visual Molecular Dynamics, http://www.ks.uiuc.edu/Research/vmd/
40. Sandia National Laboratories. LAMMPS Molecular Dynamics Simulator, http://lammps.sandia.gov/
41. http://www.ks.vasp.at/
42. Car R, Parrinello M *Phys. Rev. Lett.* **55** 2471 (1985)
43. Mott N F, Massey H S W *The Theory of Atomic Collisions* (Oxford: Clarendon Press, 1965)
44. Smirnov B M, Berry R S *Phase Transitions of Simple Systems* (Heidelberg: Springer, 2007)
45. Lindemann F A *Phys. Z.* **11** 609 (1910)
46. Etters R D, Kaelberer J *Phys. Rev. A* **11** 1068 (1975)
47. Berry R S et al. *Adv. Chem. Phys.* **70** (Pt. 2) 75 (1988)
48. Zhou Y, Karplus M, Ball K D, Berry R S *J. Chem. Phys.* **116** 2323 (2002)
49. Arrhenius S *Z. Phys. Chem.* **28** 317 (1899)
50. Conroy H, Bruner B L *J. Chem. Phys.* **47** 921 (1967)
51. Massey H S W *Rep. Prog. Phys.* **12** 248 (1949)
52. Nikitin E E, Umanskii S Ya *Theory of Slow Atomic Collisions* (Berlin: Springer, 1984) [Translated from Russian: *Neadiabaticheskie Perekhody pri Medlennykh Atomnykh Stolknoveniyakh* (Moscow: Atomizdat, 1979)]
53. Smirnov B M *Physics of Atoms and Ions* (New York: Springer, 2003)
54. Slater J C *Phys. Rev.* **34** 1293 (1929)
55. Boys S F *Proc. R. Soc. Lond. A* **200** 542 (1950)
56. Hartree D R *The Calculation of Atomic Structures* (New York: J. Wiley, 1957)
57. Eyring H *J. Chem. Phys.* **3** 107 (1935)
58. Evans M G, Polanyi M *Trans. Faraday Soc.* **31** 875 (1935)
59. Wynne-Jones W F K, Eyring H *J. Chem. Phys.* **3** 492 (1935)
60. Evans M G, Polanyi M *Trans. Faraday Soc.* **33** 448 (1937)
61. Nikitin E E *Theory of Elementary Atomic and Molecular Processes in Gases* (Oxford: Clarendon Press, 1974) [Translated from Russian: *Teoriya Elementarnykh Atomno-molekulyarnykh Protsessov v Gazakh* (Moscow: Khimiya, 1970)]
62. Laidler K J *Chemical Kinetics* (New York: Harper & Row, 1987)
63. Levine R D, Bernstein R B *Molecular Reaction Dynamics and Chemical Reactivity* (New York: Oxford Univ. Press, 1987)
64. Upadhyay S K *Chemical Kinetics and Reaction Dynamics* (New York: Springer, 2006)
65. Torello F, Dondi M G *J. Chem. Phys.* **70** 1564 (1979)
66. Partridge H et al. *J. Chem. Phys.* **99** 5951 (1993)
67. Siegbahn P, Liu B *J. Chem. Phys.* **68** 2457 (1978)
68. Westenberg A A, de Haas N *J. Chem. Phys.* **47** 1393 (1967)
69. Karplus M, Porter R N, Sharma R D *J. Chem. Phys.* **43** 3259 (1965)
70. Smirnov B M *Reference Data on Atomic Physics and Atomic Processes* (Berlin: Springer, 2008)
71. Nikitin E E *Theor. Exp. Chem.* **4** 482 (1968) [*Teor. Eksp. Khim.* **4** 751 (1968)]
72. Zembekov A A, Nikitin E E *Dokl. Akad. Nauk SSSR* **205** 1392 (1972)
73. Kondratiev V N, Nikitin E E *Gas-Phase Reactions: Kinetics and Mechanisms* (Berlin: Springer-Verlag, 1981)
74. Zewail A H *Science* **242** 1645 (1988)
75. Smirnov B M *Fundamentals of Ionized Gases* (Berlin: Wiley, 2012)
76. Berry R S *J. Chem. Phys.* **27** 1288 (1957)
77. Bond G C, Louis C, Thompson D T *Catalysis by Gold* (Singapore: World Scientific, 2006)
78. Gibbs J W *Trans. Conn. Acad. Arts Sci.* **3** 108 (1875)
79. Gibbs J W *Trans. Conn. Acad. Arts Sci.* **3** 343 (1878)
80. Gibbs J W *The Collected Works* (New York: Longmans, Green and Co., 1928)
81. ter Haar D *Elements of Thermostatistics* (New York: Holt, Rinehart and Winston, 1966)
82. ter Haar D, Wergeland H *Elements of Thermodynamics* (Reading, Mass.: Addison-Wesley Publ. Co., 1966)
83. Kubo R *Thermodynamics* (Amsterdam: North-Holland, 1968)
84. Kittel C, Kroemer H *Thermal Physics* (San Francisco: W. H. Freeman, 1980)
85. Landau L D, Lifshitz E M *Statistical Physics* Vol. 1 (Oxford: Pergamon Press, 1980) [Translated from Russian: *Statisticheskaya Fizika* Vol. 1 (Moscow: Nauka, 1976)]
86. Stowe K *Introduction to Statistical Physics and Thermodynamics* (New York: Wiley, 1984)
87. Callen H *Thermodynamics and Introduction to Thermostatics* (New York: Wiley, 1984)
88. Smirnov B M *Phys. Usp.* **44** 1229 (2001) [*Usp. Fiz. Nauk* **171** 1291 (2001)]
89. Kittel Ch *Introduction to Solid State Physics* (New York: Wiley, 1986)
90. Smirnov B M *JETP* **85** 1010 (1997) [*Zh. Eksp. Theor. Fiz.* **112** 1847 (1997)]
91. Smirnov B M *Phys. Scripta* **58** 595 (1998)
92. Smirnov B M *Clusters and Small Particles: in Gases and Plasmas* (New York: Springer, 2000)
93. Smirnov B M *Inorg. Mater.* **35** 562 (1999)
94. Berry R S, Smirnov B M, in *Nucleation Theory and Applications* (Eds J W P Schmelzer, G Röpke, V B Priezzhev) (Dubna: JINR, 2002) p. 340
95. Mackay A L *Acta Cryst.* **15** 916 (1962)
96. Wales D J, Berry R S *J. Chem. Phys.* **92** 4283 (1990)
97. Berry R S, Jellinek J, Natanson G *Phys. Rev. A* **30** 919 (1984)
98. Jellinek J, Beck T L, Berry R S *J. Chem. Phys.* **84** 2783 (1986)
99. Berry R S *Chem. Rev.* **93** 2379 (1993)
100. Kunz R E, Berry R S *Phys. Rev. E* **49** 1895 (1994)
101. Berry R S, in *Theory of Atomic and Molecular Clusters* (Ed. J Jellinek) (Berlin: Springer, 1999) p. 1
102. Davis H L, Jellinek J, Berry R S *J. Chem. Phys.* **86** 6456 (1987)
103. Berry R S, Smirnov B M *JETP* **100** 1129 (2005) [*Zh. Eksp. Teor. Fiz.* **127** 1282 (2005)]
104. Berry R S, Smirnov B M *Phys. Usp.* **48** 345 (2005) [*Usp. Fiz. Nauk* **175** 367 (2005)]
105. Berry R S, Smirnov B M *Low Temp. Phys.* **35** 256 (2009) [*Fiz. Nizk. Temp.* **35** 339 (2009)]
106. Berry R S, Smirnov B M *J. Chem. Phys.* **130** 064302 (2009)
107. Bixon M, Jortner J *J. Chem. Phys.* **91** 1631 (1989)
108. Wales D J et al. *Adv. Chem. Phys.* **115** 1 (2000)
109. Kunz R E, Berry R S *Phys. Rev. Lett.* **71** 3987 (1993)
110. Wales D J *Chem. Phys. Lett.* **166** 419 (1990)
111. Braier P A, Berry R S, Wales D J *J. Chem. Phys.* **93** 8745 (1990)
112. Labastie P, Whetten R L *Phys. Rev. Lett.* **65** 1567 (1990)
113. Cheng H-P, Berry R S *MRS Symp. Proc.* **206** 241 (1991)
114. Cheng H-P, Berry R S *Phys. Rev. A* **45** 7969 (1992)
115. Doye J P K, Wales D J *J. Chem. Phys.* **102** 9659 (1995)
116. Finnis M W, Sinclair J E *Philos. Mag. A* **50** 45 (1984)
117. Sutton A P, Chen J *Philos. Mag. Lett.* **61** 139 (1990)
118. Freeman D L, Doll J D *J. Chem. Phys.* **82** 462 (1985)
119. Arslan H, Güven M H *New J. Phys.* **7** 60 (2005)
120. Garzón I L, Jellinek J *Z. Phys. D* **20** 235 (1991)
121. Garzón I L, Jellinek J *Z. Phys. D* **26** 316 (1993)
122. Neirotti J P et al. *J. Chem. Phys.* **112** 10340 (2000)
123. Calvo F et al. *J. Chem. Phys.* **112** 10350 (2000)
124. Lee Y J et al. *J. Comput. Chem.* **21** 380 (2000)
125. Carignano M A *Chem. Phys. Lett.* **361** 291 (2002)
126. Sebetci A, Guvenc Z B *Modelling Simul. Mater. Sci. Eng.* **12** 1131 (2004)
127. Doye J P K, Wales D J *New J. Chem.* **22** 733 (1998)

128. Koskinen P et al. *New J. Phys.* **8** 9 (2006)
129. Gafner S L, Gafner Yu Ya *JETP* **107** 712 (2008) [*Zh. Eksp. Teor. Fiz.* **134** 831 (2008)]
130. Gafner S L, Redel L V, Gafner Yu Ya *JETP* **108** 784 (2009) [*Zh. Eksp. Teor. Fiz.* **135** 899 (2009)]
131. Gafner Yu Ya, Gafner S L, Chepkasov I V *JETP* **111** 608 (2010) [*Zh. Eksp. Teor. Fiz.* **138** 687 (2010)]
132. Daw M S, Baskes M I *Phys. Rev. Lett.* **50** 1285 (1983)
133. Daw M S, Baskes M I *Phys. Rev. B* **29** 6443 (1984)
134. Lee Y J et al. *Phys. Rev. Lett.* **86** 999 (2001)
135. Coquet R, Howard K L, Willock D J *Chem. Soc. Rev.* **37** 2046 (2008)
136. van Lenthe E, Baerends E J, Snijders J G *J. Chem. Phys.* **99** 4597 (1993)
137. van Lenthe E, Baerends E J, Snijders J G *J. Chem. Phys.* **101** 9783 (1994)
138. Pyykkö P *Chem. Rev.* **88** 563 (1988)
139. Pyykkö P *Angew. Chem. Int. Ed.* **43** 4412 (2004)
140. Pyykkö P *Inorg. Chim. Acta* **358** 4113 (2005)
141. Philipsen P H T, Baerends E J *Phys. Rev. B* **61** 1773 (2000)
142. Berry R S, Smirnov B M *Phys. Usp.* **52** 137 (2009) [*Usp. Fiz. Nauk* **179** 147 (2009)]
143. Häberlen O D et al. *J. Chem. Phys.* **106** 5189 (1997)
144. Doye J P K, Wales D J *J. Chem. Soc. Faraday Trans.* **93** 4233 (1997)
145. Wilson N T, Johnston R L *Eur. Phys. J. D* **12** 161 (2000)
146. Darby S et al. *J. Chem. Phys.* **116** 1536 (2002)
147. Wang J, Wang G, Zhao J *Phys. Rev. B* **66** 035418 (2002)
148. Oviedo J, Palmer R E *J. Chem. Phys.* **117** 9548 (2002)
149. Johansson M P et al. *Phys. Rev. A* **77** 053202 (2008)
150. Li J et al. *Science* **299** 864 (2003)
151. Häkkinen H et al. *J. Phys. Chem. A* **107** 6168 (2003)
152. Furche F et al. *J. Chem. Phys.* **117** 6982 (2002)
153. Glib S et al. *J. Chem. Phys.* **116** 4094 (2002)
154. Xiao Li et al. *J. Chem. Phys.* **124** 114309 (2006)
155. Fielicke A et al. *Phys. Rev. Lett.* **93** 023401 (2004)
156. Fielicke A, von Helden G, Meijer G *Eur. Phys. J. D* **34** 83 (2005)
157. Gruene P et al. *Science* **321** 674 (2008)
158. Komoda T *Jpn. J. Appl. Phys.* **7** 27 (1968)
159. Buffat P-A et al. *Faraday Discuss.* **92** 173 (1991)
160. Marks L D *Rep. Prog. Phys.* **57** 603 (1994)
161. Ascencio J A et al. *Surf. Sci.* **396** 349 (1998)
162. Ascencio J A, Pérez M, José-Yacamán M *Surf. Sci.* **447** 73 (2000)
163. Koga K, Sugawara K *Surf. Sci.* **529** 23 (2003)
164. Häkkinen H et al. *Phys. Rev. Lett.* **93** 093401 (2004)
165. Koga K, Ikeshoji T, Sugawara K *Phys. Rev. Lett.* **92** 115507 (2004)
166. Suzdalev I P *Nanotekhnologiya: Fiziko-Khimiya Nanoklasterov, Nanostruktur i Nanomaterialov* (Nanotechnology: Physical Chemistry of Nanoclusters, Nanostructures and Nanomaterials) (Moscow: KomKniga, 2006)
167. Makarov G N *Phys. Usp.* **51** 319 (2008) [*Usp. Fiz. Nauk* **178** 337 (2008)]
168. Makarov G N *Phys. Usp.* **53** 179 (2010) [*Usp. Fiz. Nauk* **185** 1079 (2010)]
169. Natanson G, Amar F, Berry R S *J. Chem. Phys.* **78** 399 (1983)
170. Smirnov B M *Phys. Usp.* **37** 1079 (1994) [*Usp. Fiz. Nauk* **164** 1165 (1994)]
171. Berry R S, Smirnov B M *J. Chem. Phys.* **114** 6816 (2001)
172. Berry R S, Smirnov B M *J. Non-Cryst. Solids* **351** 1543 (2005)
173. Arslan H, Güven M H *Acta Phys. Slovac.* **56** 511 (2006)
174. Yildirim E K, Atis M, Guvenc Z B *Phys. Scripta* **75** 111 (2007)
175. Beck T L, Jellinek J, Berry R S *J. Chem. Phys.* **87** 545 (1987)
176. Berry R S, Smirnov B M *Nanomech. Sci. Technol. Int. J.* **3** 167 (2012)
177. Fogler H S *Elements of Chemical Reaction Engineering* (Englewood Cliffs, N.J.: Prentice-Hall, 1992)
178. Atkins P W *Physical Chemistry* (New York: W.H. Freeman, 1994)
179. Boreskov G K *Heterogeneous Catalysis* (Hauppauge, N.Y.: Nova Science Publ., 2003)
180. Ertl G et al. (Eds) *Handbook of Heterogeneous Catalysis* (Weinheim: Wiley, 2008)
181. Rothenberg G *Catalysis: Concepts and Green Applications* (Weinheim: Wiley, 2008)
182. Kolasinski K W *Surface Science: Foundations of Catalysis and Nanoscience* (Weinheim: Wiley, 2008)
183. http:/www.chemguide.co.uk/physical/catalysis
184. http://en.wikipedia.org/wiki/Heterogeneous_catalysis
185. Bond G C *Catalysis by Metals* (London: Academic Press, 1962)
186. Ponec V, Bond G C *Catalysis by Metals and Alloys* (Amsterdam: Elsevier, 1995)
187. Haruta M *CATTECH* **6** 102 (2002)
188. Judai K et al. *Int. J. Mass Spectrom.* **229** 99 (2003)
189. Judai K et al. *J. Am. Chem. Soc.* **126** 2732 (2004)
190. Kittel Ch *Thermal Physics* (New York: Wiley, 1970)
191. Bligaard T et al. *J. Catal.* **224** 206 (2004)
192. Berry R S, Smirnov B M *J. Phys. Chem. A* **113** 14220 (2009)
193. Rainer D R et al. *J. Catal.* **167** 234 (1997)
194. Piccolo L, Henry C R *Appl. Surf. Sci.* **162–163** 670 (2000)
195. Piccolo L, Henry C R *J. Mol. Catal. A* **167** 181 (2001)
196. Heiz U, Landman U (Eds) *Nanocatalysis* (Berlin: Springer, 2007)
197. Moshfegh A Z *J. Phys. D* **42** 233001 (2009)
198. Gellman A J, Shukla N *Nature Mater.* **8** 87 (2009)
199. Haruta M *Catal. Today* **36** 153 (1997)
200. Haruta M et al. *Chem. Lett.* **16** 405 (1987)
201. Haruta M et al. *J. Catal.* **115** 301 (1989)
202. Wigner E, Seitz F *Phys. Rev.* **46** 509 (1934)
203. Wigner E *Phys. Rev.* **46** 1002 (1934)
204. Haruta M *Chem. Record* **3** 75 (2003)
205. Bondzie V A, Parker S C, Campbell C T *Catal. Lett.* **63** 143 (1999)
206. Chang C M, Chou M Y *Phys. Rev. Lett.* **93** 133401 (2004)
207. Herzing A A et al. *Science* **321** 1331 (2008)
208. Tian N et al. *Science* **316** 732 (2007)
209. Ueda A, Haruta M *Resources Environment* **28** 1035 (1992)
210. Funazaki N et al. *Sensors Actuators B* **14** 536 (1993)
211. Corti C W, Holliday R J, Thompson D T *Appl. Catal.* **291** 253 (2005)
212. Biswas P C et al. *J. Electroanalyt. Chem.* **381** 167 (1995)
213. Zhang J et al. *Science* **315** 220 (2007)
214. Winther-Jensen B et al. *Science* **321** 671 (2008)
215. Hutchings G J *Gold Bull.* **37** 3 (2004)
216. Christensen C H, Nørskov J K *Science* **327** 278 (2010)
217. Corma A, Garcia H *Chem. Soc. Rev.* **37** 2096 (2008)
218. Biella S, Prati L, Rossi M *J. Catal.* **206** 242 (2002)
219. Christensen C H et al. *Angew. Chem. Int. Ed.* **45** 4648 (2006)
220. Sinha A K et al. *Top Catal.* **29** (3–4) 95 (2004)
221. Kishi K, Daté M, Haruta M *Surf. Sci. Lett.* **486** L475 (2001)
222. Landau L D, Lifshitz E M *Quantum Mechanics. Non-Relativistic Theory* (Oxford: Pergamon Press, 1977) [Translated from Russian: *Kvantovaya Mekhanika. Nerelyativistskaya Teoriya* (Moscow: Nauka, 1974)]
223. Lide D R (Ed.-in-Chief) *Handbook of Chemistry and Physics* 86th ed. (London: CRC Press, 2003–2004)
224. Bond G C, Louis C, Thompson D T *Catalysis by Gold* (London: Imperial College Press, 2006)
225. Berry R S, Smirnov B M *JETP* **113** 907 (2011) [*Zh. Eksp. Teor. Fiz.* **140** 1043 (2011)]
226. Berry R S, Smirnov B M *Europhys. Lett.* **97** 63003 (2012)
227. Taylor K J et al. *J. Chem. Phys.* **96** 3319 (1992)
228. Smirnov B M *Cluster Processes in Gases and Plasmas* (Weinheim: Wiley-VCH, 2010)
229. Berry R S, Smirnov B M *Phys. Rep.* **527** 205 (2013)
230. Haruta M, Daté M *Appl. Catal. A* **222** 427 (2001)
231. Min B K et al. *J. Phys. Chem. B* **110** 19833 (2006)
232. Min B K, Friend C M *Chem. Rev.* **107** 2709 (2007)
233. Finch R M et al. *Phys. Chem. Chem. Phys.* **1** 485 (1999)
234. Kahlich M J, Gasteiger H A, Behm R J *J. Catal.* **182** 430 (1999)
235. Avgouropoulos G et al. *Catal. Lett.* **73** 33 (2001)
236. Golunski S et al. *Catal. Today* **72** 107 (2002)
237. Avgouropoulos G et al. *Catal. Today* **75** 157 (2002)
238. Landon P et al. *J. Mater. Chem.* **16** 199 (2006)
239. Haruta M et al. *Stud. Surf. Sci. Catal.* **44** 33 (1989)
240. Haruta M *Catal. Surv. Jpn.* **1** 61 (1997)
241. Zanella R et al. *J. Phys. Chem. B* **106** 7634 (2002)
242. Zanella R, Delannoy L, Louis C *Appl. Catal. A* **291** 62 (2005)
243. Zanella R, Louis C *Catal. Today* **107–108** 768 (2005)
244. Li W-C, Comotti M, Schüth F *J. Catal.* **237** 190 (2006)
245. Comotti M et al. *J. Am. Chem. Soc.* **128** 917 (2006)
246. Guzman J, Carrettin S, Corma A *J. Am. Chem. Soc.* **127** 3286 (2005)
247. Sakurai H et al. *Appl. Catal. A* **291** 179 (2005)
248. Häkkinen H et al. *Angew. Chem. Int. Ed.* **42** 1297 (2003)

249. Sanchez A et al. *J. Phys. Chem. A* **103** 9573 (1999)
250. Yoon B et al. *Science* **307** 403 (2005)
251. Coquet R et al. *J. Mater. Chem.* **16** 1978 (2006)
252. Harding C et al. *J. Am. Chem. Soc.* **131** 538 (2009)
253. Ricci D et al. *Phys. Rev. Lett.* **97** 036106 (2006)
254. Sterrer M et al. *Phys. Rev. Lett.* **98** 096107 (2007)
255. Zhang C, Yoon B, Landman U *J. Am. Chem. Soc.* **129** 2228 (2007)
256. Perdew J P et al. *Phys. Rev. B* **46** 6671 (1992)
257. Perdew J P, Burke K, Ernzerhof M *Phys. Rev. Lett.* **77** 3865 (1996)
258. Stampfl C, Scheffler M *Phys. Rev. Lett.* **78** 1500 (1997)
259. Alavi A et al. *Phys. Rev. Lett.* **80** 3650 (1998)
260. Eichler A, Hafner J *Surf. Sci.* **433 – 435** 58 (1999)
261. Sanchez A et al. *J. Phys. Chem. A* **103** 9573 (1999)
262. Mavrikakis M, Stoltze P, Nørskov J K *Catal. Lett.* **64** 101 (2000)
263. Zhang C J, Hu P *J. Am. Chem. Soc.* **122** 2134 (2000)
264. Hammer B *J. Catal.* **199** 171 (2001)
265. Castellarin Cudia C et al. *Phys. Rev. Lett.* **87** 196104 (2001)
266. Zhang C J, Hu P, Alavi A *J. Chem. Phys.* **114** 8113 (2001)
267. Lopez N, Nørskov J K *J. Am. Chem. Soc.* **124** 11262 (2002)
268. Liu Z-P, Hu P, Alavi A *J. Am. Chem. Soc.* **124** 14770 (2002)
269. Liu Z-P et al. *Phys. Rev. Lett.* **91** 266102 (2003)
270. Molina L M, Hammer B *Phys. Rev. Lett.* **90** 206102 (2003)
271. Mills G, Gordon M S, Metiu H *J. Chem. Phys.* **118** 4198 (2003)
272. Yoon B, Häkkinen H, Landman U *J. Phys. Chem. A* **107** 4066 (2003)
273. Xu Y, Mavrikakis M *J. Phys. Chem. B* **107** 9298 (2003)
274. Molina L M, Hammer B *Phys. Rev. B* **69** 155424 (2004)
275. Molina L M, Hammer B *Appl. Catal. A* **291** 21 (2005)
276. Chen Y, Crawford P, Hu P *Catal. Lett.* **119** 21 (2007)
277. Heiz U, Bernhardt T M, Landman U, in *Nanocatalysis* (Eds U Heiz, U Landman) (Berlin: Springer, 2007)
278. Kong L, Bischoff F A, Valeev E F *Chem. Rev.* **112** 75 (2012)
279. Moseler M, Häkkinen H, Landman U *Phys. Rev. Lett.* **89** 176103 (2002)
280. Cleveland C L, Luedtke W D, Landman U *Phys. Rev. Lett.* **81** 2036 (1998)
281. Chushak Y G, Bartell L S *J. Phys. Chem. B* **105** 11605 (2001)
282. Nam H-S et al. *Phys. Rev. Lett.* **89** 275502 (2002)
283. Haruta M *Catal. Today.* **36** 153 (1997)
284. Turner M et al. *Nature* **454** 981 (2008)
285. Goodman D W *Nature* **454** 948 (2008)
286. Valden M, Lai X, Goodman D W *Science* **281** 1647 (1998)
287. Schubert M M et al. *J. Catal.* **197** 113 (2001)
288. Lopez N et al. *J. Catal.* **223** 232 (2004)
289. Grunwaldt J-D, Baiker A *J. Phys. Chem. B* **103** 1002 (1999)
290. Dekkers M A P, Lippits M J, Nieuwenhuys B E *Catal. Lett.* **56** 195 (1998)
291. Dekkers M A P, Lippits M J, Nieuwenhuys B E *Catal. Today* **54** 381 (1999)
292. Bond G C, Thompson D J *Gold Bull.* **33** 41 (2000)
293. Liu Z-P, Hu P, Alavi A *J. Am. Chem. Soc.* **124** 14770 (2002)
294. Salisbury B E, Wallace W T, Whetten R L *Chem. Phys.* **262** 131 (2000)
295. Wallace W T, Whetten R L *J. Phys. Chem. B* **104** 10964 (2000)
296. Wahlström E et al. *Phys. Rev. Lett.* **90** 026101 (2003)
297. Lopez N et al. *J. Catal.* **225** 86 (2004)
298. Chen M, Goodman D W *Acc. Chem. Res.* **39** 739 (2006)
299. Roberts J T, Capote A J, Madix R J *Surf. Sci.* **253** 13 (1991)
300. Chan A S Y, Deiner L J, Friend C M *J. Phys. Chem. B* **106** 13318 (2002)
301. Webb M J, Driver S M, King D A *J. Phys. Chem. B* **108** 1955 (2004)
302. Schaub R et al. *Phys. Rev. Lett.* **87** 266104 (2001)
303. Kung H H, Kung M C, Costello C K *J. Catal.* **216** 425 (2003)
304. Sanchez-Castillo M A et al. *Angew. Chem. Int. Ed.* **43** 1140 (2004)
305. Daté M et al. *Angew. Chem. Int. Ed.* **43** 2129 (2004)
306. Costello C K et al. *J. Phys. Chem. B* **108** 12529 (2004)
307. Liu L M et al. *J. Am. Chem. Soc.* **128** 4017 (2006)
308. Bongiorno A, Landman U *Phys. Rev. Lett.* **95** 106102 (2005)
309. Lakhno V D *Clusters in Physics, Chemistry and Biology* (Moscow – Izhevsk: RKhD, 2001)